TECHNICAL REPORT: MATERIALS AND CHEMISTRY

INVESTIGATION OF STRUCTURAL PROPELLANT SYSTEMS

LMSD-895015

DECEMBER 1960

Lockheed
MISSILES and SPACE DIVISION
LOCKHEED AIRCRAFT CORPORATION · SUNNYVALE, CALIF.

TECHNICAL REPORT: MATERIALS AND CHEMISTRY

INVESTIGATION OF STRUCTURAL PROPELLANT SYSTEMS

BY

A. HOLMES, H. T. HSIA, H. P. MARSHALL,
A.C. MILLER, AND PAUL NOBLE, JR.

LMSD-895015 DECEMBER 1960

WORK CARRIED OUT AS PART OF THE LOCKHEED GENERAL RESEARCH PROGRAM

Lockheed

MISSILES and SPACE DIVISION

LOCKHEED AIRCRAFT CORPORATION • SUNNYVALE, CALIF.

NOTICE

QUALIFIED REQUESTERS MAY OBTAIN COPIES OF THIS REPORT FROM THE ARMED SERVICES TECHNICAL INFORMATION AGENCY (ASTIA). DEPARTMENT OF DEFENSE CONTRACTORS MUST BE ESTABLISHED FOR ASTIA SERVICES, OR HAVE THEIR NEED-TO-KNOW CERTIFIED BY THE MILITARY AGENCY COGNIZANT OF THEIR CONTRACT.

THIS REPORT HAS BEEN RELEASED TO THE OFFICE OF TECHNICAL SERVICES, DEPARTMENT OF COMMERCE, WASHINGTON 25, D.C., FOR SALE TO THE GENERAL PUBLIC.

DISTRIBUTION OF THIS REPORT TO OTHERS SHALL NOT BE CONSTRUED AS GRANTING OR IMPLYING A LICENSE TO MAKE, USE, OR SELL ANY INVENTION DESCRIBED HEREIN UPON WHICH A PATENT HAS BEEN GRANTED OR A PATENT APPLICATION FILED BY LOCKHEED AIRCRAFT CORPORATION. NO LIABILITY IS ASSUMED BY LOCKHEED AS TO INFRINGEMENT OF PATENTS OWNED BY OTHERS.

FOREWORD

This report presents an analysis of the merits of utilizing metal structures in solid propellants. The analysis was carried out jointly by the Propulsion Research and the Structures Departments as part of the LMSD General Research Program.

SUMMARY

Based on the results of a previous study, a structural propellant concept has been developed which would permit utilization of high-energy propellants, with marginal physical properties, in rocket motors. This report presents the results of a program undertaken to exploit this new concept and to evaluate the problems associated with its implementation. These problems include:

- The evaluation of burning rates of structural propellants
- The determination of structural aspects of reinforced propellants
- The development and testing of propellant grains

The studies completed in this program have yielded the following results:

(1) The burning rate of propellant strands containing metal laminations is increased by a factor of three or more over that of strands without laminations. In general, the magnitude of the increase in dependent upon:

- The thermal conductivity of the metal – the higher the conductivity, the higher the resultant burning rate
- The thickness of the lamination – the thicker laminations giving higher burning rates, although a maximum is apparently reached and thicker laminations then reduce the burning rates
- The number of laminations – burning rates increase to a maximum value as the number of laminations increase, and the use of additional laminations causes a burning rate reduction

A theoretical analysis of these phenomena was also undertaken in an attempt to predict the effect of different metal laminations on the burning rate of the propellant.

(2) From theoretical evaluation of the use of structural elements in propellant grains, it was concluded that incorporation of proper reinforcement into propellant grains can produce a 50 to 75 percent reduction in propellant stress. In general, the extent of stress reduction increases with increasing values of the ratio of elastic modulus of the reinforcing to elastic modulus of the propellant material. However, use of large reinforcing elements may act as a source of stress concentration, or if expansion coefficients of reinforcing and propellant materials are widely divergent, delamination may occur with large temperature changes.

(3) The low binder content of high-energy propellants causes poor flow characteristics. This property, coupled with exceptional energy release by the propellant, necessitates that new handling procedures for preparation of burning strands and propellant grains be developed. During this study, an isostatic pressure technique for forming propellant strands, and a remotely operated propellant-grain forming procedure were established.

CONTENTS

LIST OF ILLUSTRATIONS

LIST OF TABLES

Section 1
INTRODUCTION

The development of high-energy propellants (specific impulse in excess of 300 lb-sec/lb) has been a major objective of the Propulsion Research effort. In the initial studies, it was found that incorporation of normal amounts of a binder in the propellant system would reduce the energy of the system to such an extent that the high-energy objective could not be achieved. Accordingly, propellant systems were sought which contained minimal amounts of binder. It was immediately evident that the physical properties (tensile strength, elongation, etc.) of such a system would be very poor and that significant problems would be presented in adapting the propellant for use in conventional rocket motors.

Accordingly, a structural propellant concept was born which would permit utilization of the high-energy propellants in rocket motors. In this concept, a structural element is incorporated into the propellant so that loads imposed by rocket motor flight and handling are distributed uniformly throughout the propellant grains.

The present program on structured propellants was therefore undertaken to exploit the new concept and to evaluate further problems associated with structural propellant usage. The program has been divided into three phases:

(1) Evaluation of burning rates of propellants containing structural elements
(2) Determination of structural aspects of reinforcements in propellant grains
(3) Development and testing of propellant grains

Although new and difficult problems were presented in each of these phases, considerable progress has been achieved; the results are reported in the following sections.

Section 2

EVALUATION OF BURNING RATES OF PROPELLANTS CONTAINING STRUCTURAL ELEMENTS

2.1 INTRODUCTION

It has previously been established that the burning rate of propellants could be altered by the incorporation of metal wires into the propellant. However, the effects of metal laminates such as would exist in a structural propellant have not been investigated. The purpose of this program was to determine the effects of various metals and of different thicknesses of the metals on the burning rates of the propellant. Since the program was designed to establish basic principles, only relatively simple propellants which would permit maximum experimentation were utilized.

2.2 PROPELLANT SYSTEM

The propellant ingredients selected for this study were composed of ammonium perchlorate and powdered aluminum. In addition, a binder system was required which would permit the use of casting techniques for preparing propellant systems with high solids content. Epoxy systems were best suited for this propellant, both because of their good adhesive properties and simplified handling techniques. A low-viscosity, flexibilized epoxy system was developed which was quite satisfactory for the preparation of propellant strands containing 80 percent solids (ammonium perchlorate and powdered aluminum). The principal difficulty with the formulation developed previously was the unusually high burning rates of some preliminary strands (ca., 11 in/sec). This problem was traced to the boron trifluoride-amine complex used as the curing agent. It was found that this curing agent produced strands with varying degrees of porosity, which apparently resulted from a slow reaction of the amine portion of the curing agent with the ammonium perchlorate which yielded ammonia gas. This problem

was overcome, however, by use of maleic anhydride as the curing agent and good strands were obtained; the burning rate and burning characteristics were comparable to commercially produced propellants.

The formulations used in the study of the effects of metal structures on burning rates are given in Table 2-1. Two formulations were studied: one with the stoichiometric ratio of powdered aluminum to ammonium perchlorate (62 NH_4ClO_4 to 38 Al), the other with less powdered aluminum (85 NH_4ClO_4 to 15 Al). These formulations are based upon a solids to resin ratio of 80/20, which was considered adequate for a study of relative effects. This system, containing 20 percent resin, yields a cast propellant with a density of 1.88 g/cm^3, which is greater than 90 percent of the predicted density.

Some work with a solids to resin ratio of 90/10 was also carried out, but compression molding was necessary to achieve propellant densities approaching those theoretically possible. An indication of the effect of pressure upon the density of compressed pellets of a propellant at 90 percent solids (NH_4ClO_4 to Al ratio of 62/38) is given in Table 2-2. At pressures exceeding 10,000 psi, the density exceeds 90 percent of that calculated on the basis of 10 percent resin; however, at these pressures some resin is forced out, thereby giving propellant samples with a final resin content of only 6 to 7 percent. For the preparation of propellant mixtures containing only 10 percent resin, uniform blending is a problem. The use of volatile solvents (e.g., methylene chloride) followed by in vacuo removal of the solvent during mixing usually gives a good, uniform mix.

Attempts to prepare suitable propellants of 90 percent solids using other binders were not successful. Polyurethane resins could probably be used, but the principal difficulties were avoiding water (which causes bubbles) and adequate mixing and degassing at the high solids content. Polyisobutylene did not lend itself to compression, requiring a much higher pressure to attain significant densities. Also, its adhesion to metals is poor at elevated temperatures. Polyvinyl acetate could not be compressed unless excessive amounts of plasticizer were used; this also resulted in poor adhesion.

Table 2-1

PROPELLANT FORMULATIONS

		% by wt.
Formulation I		
	Ammonium Perchlorate[a]	49.6
	Aluminum Powder[b]	30.4
	Resin*	20.0
Formulation II		
	Ammonium Perchlorate[a]	68.0
	Aluminum Powder[b]	12.0
	Resin*	20.0

*Resin: 100 pts. by wt. Epon 815[c]; 50 pts. by wt Araldite RD-2[d]; 50 pts. by wt. Cardolite NC 513[e]; 20 pts. by wt. maleic anhydride, plus 1 percent Triton X-100[f]

(a) B. F. Goodrich Co.

(b) Alcoa No. 123

(c) Shell Chemical Corp.

(d) Ciba, Inc.

(e) Minn. Mining & Mfg. Co.

(f) Rohm and Haas Co.

Table 2-2

PROPELLANT[a] DENSITIES AS A FUNCTION OF PRESSING PRESSURE

No.	Pressure on Sample[b] (psi)	Density[c] (g/cm^3)
1	3,070	(d)
2	6,140[e]	1.86
3	9,210[e]	1.97
4	21,400[e]	2.05
5	25,600[e]	2.02
6	30,700[e]	2.06

(a) Propellant formulation at 90 percent solids, Al to NH_4ClO_4 ratio of 38/62; 10 percent resin formulated as indicated in Table 2-1

(b) Area of pellet: 0.307 in^2

(c) Theoretical density calculated: 2.12 g/cm^3

(d) Sample fell apart

(e) Loss of resin due to pressing

2.3 CASTING PROPELLANT STRANDS

The propellant strands were cast in 1/2 -in. -aluminum channel molds coated with silicone mold-release lubricant and then lined with cast Teflon film (1 mil). The molds were closed by cementing 1/4-in. plywood squares over the ends. In cases where strips of metal were to be laminated longitudinally through the strand, the plywood ends were slotted and the metal held firmly in place prior to casting.

The propellant, prepared according to the desired formulation (Table 2-1), was mixed with an ordinary laboratory stirrer (rotary) in a three-necked, round-bottomed flask fitted with vacuum takeoff. The dry components, except the curing agent, were mixed and degassed, followed by addition of the heated (70°C) resin containing the maleic anhydride. This mixture was stirred with intermittent degassing at a temperature of 80° to 85°C until well blended—usually about 30 min. The mixture was poured immediately into preheated molds (any trapped air bubbles were removed by tapping) and cured in an oven overnight at 85°C.

A typical mold and strand are shown in Fig. 2-1.

2.4 PROPERTIES OF THE CAST STRANDS

Although the burning characteristics of these propellants were of primary concern, other studies were made to obtain as much information as possible, especially regarding those properties that could possibly affect rates of burning.

The adhesion of the binders to the metal is an important factor; areas of poor adhesion of the binders to the metal is an important factor; areas of poor adhesion or delamination during burning would expose new surfaces and greatly increase the burning rate. Before placing it in the mold, the metal was cleaned very carefully in an acidic dichromate solution. Several of the finished strands containing metal laminated strips were examined for adhesive failure; excellent bonding was observed in all cases

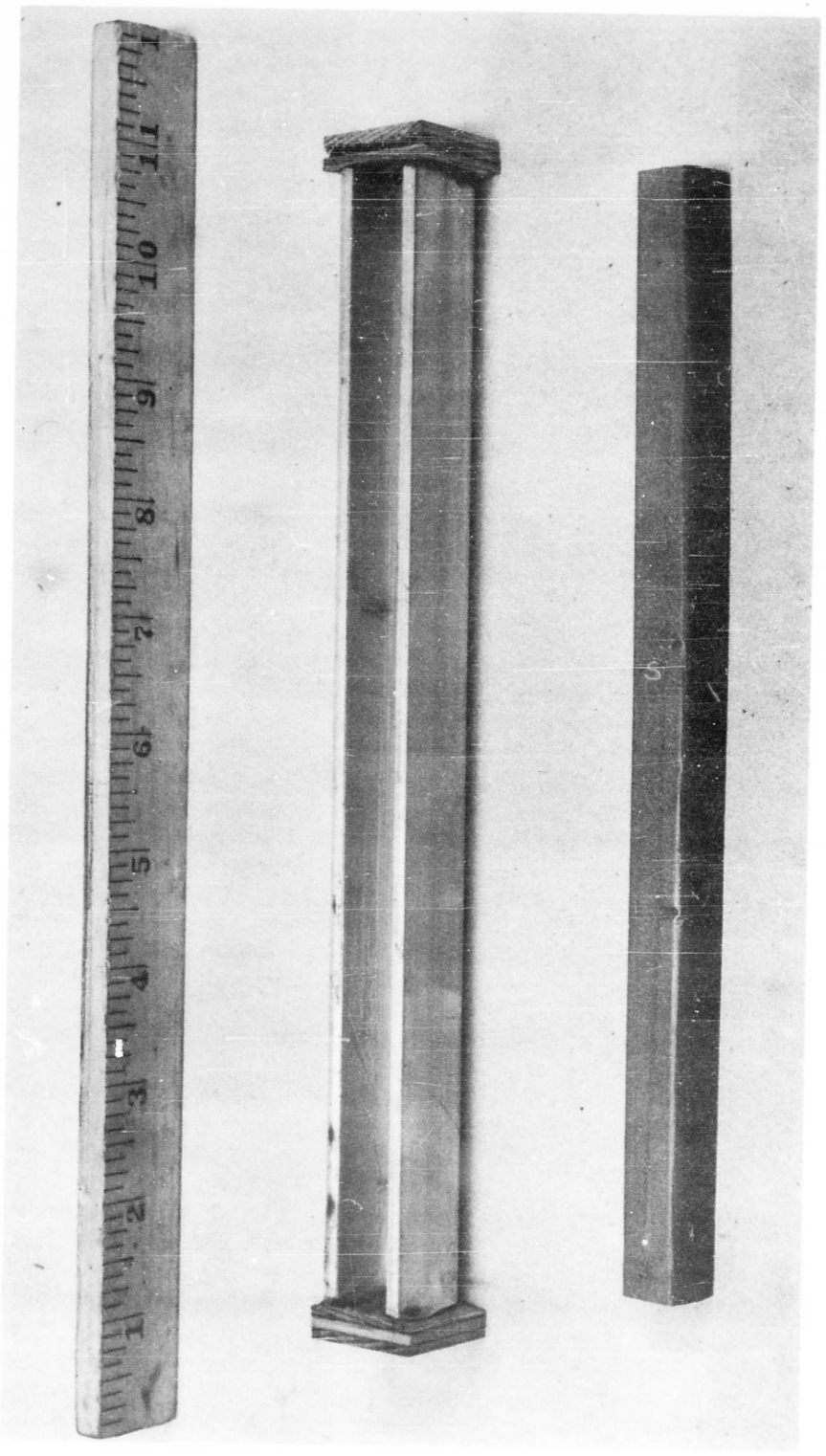

Fig. 2-1 Typical Propellant Mold and Strand

noted. In addition, the strands were free from voids, except at outside edges, and quite uniform in texture.

Some of the strands prepared from Formulation II (NH_4ClO_4 to Al ratio of 85/15) (Table 2-1) containing the heavier gage metal exhibited cracks normal to the face of the metal. In Formulation I (NH_4ClO_4 to Al ratio of 62/38), no cracks were observed.

The strands were carefully coated with three coats of polyvinyl chloride-polyvinyl acetate copolymer and one coat of silicone grease, prior to actual burning, to inhibit burning on the side of the strand.

Some physical properties of the propellant strands are given in Section 3.

2.5 BURNING-RATE APPARATUS

A special strand burner employing a fast-response, gas-bleeding system is capable of burning the large strands (up to 1/2 in. by 1/2 in. by 6 in.). However, difficulty in reproducing burning rates (discussed below) necessitated some modification. Figure 2-2 shows a strand in place (not wired) on the modified strand holder, which was covered with a formica sheet to aid in preventing electrical shorts caused by build-up of metal fragments around the insulated terminals.

The burning operation can be explained by referring to Fig. 2-2. The terminals on the left are insulated (hot), and those on the right are grounded to the holder. Wires are threaded through small holes (at measured distances) in the strand, and then attached to the appropriate terminals. The strand is ignited (a small piece of aluminized propellant is used to ignite the surface of the strand) by applying a potential across the top pair of terminals. The burning continues down the strand (top to bottom in Fig. 2-2) severing the wires and breaking the electrical circuit between the terminals. Discontinuity of the electrical circuit at the second set of terminals starts two clocks. Discontinuity of the electrical circuit at third set of terminals stops one of the clocks,

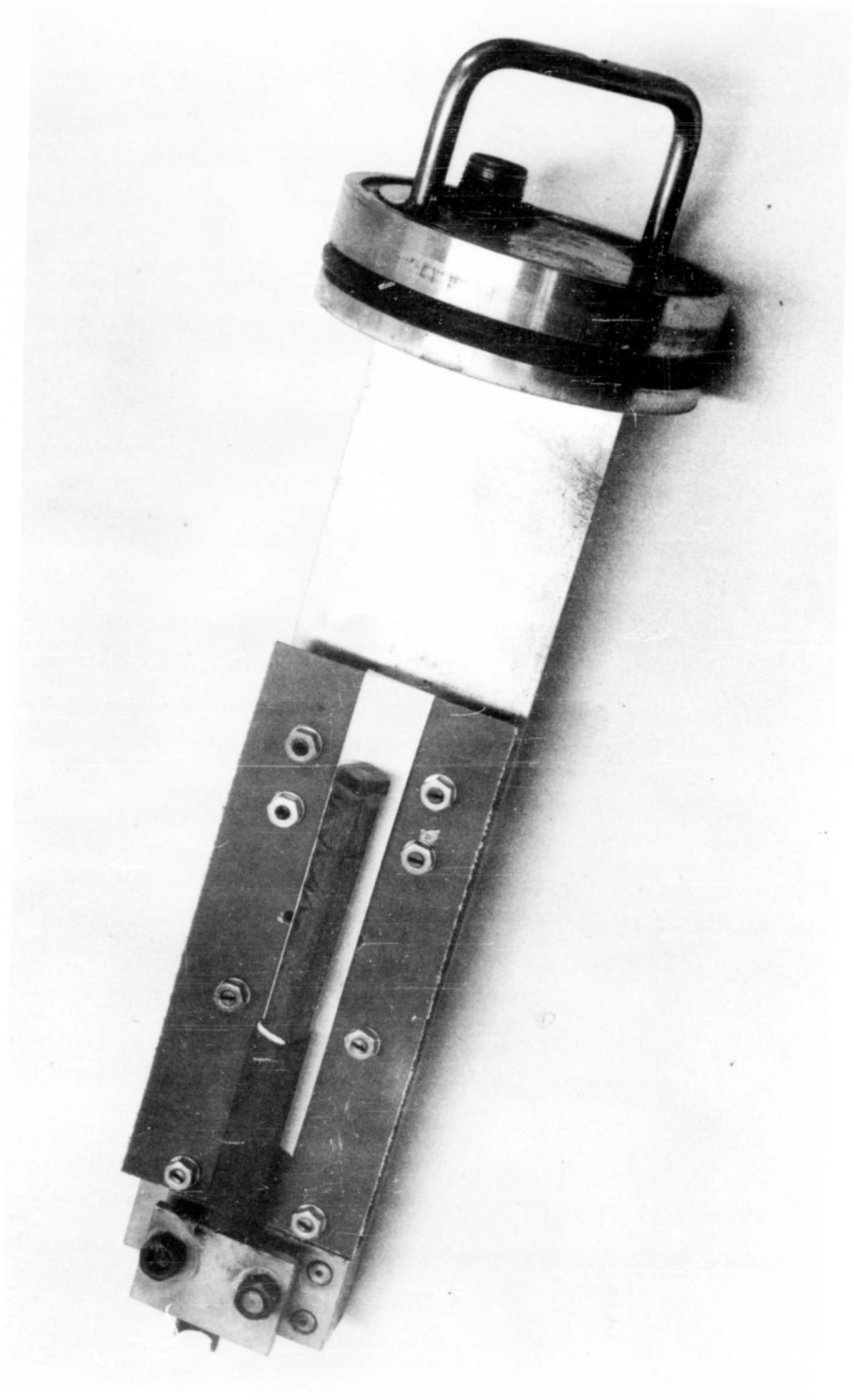

Fig. 2-2 Modified Strand Holder With Propellant Strand in Place

and at the fourth set of terminals it stops the other clock. A burning rate is then calculated by using the known distance between the wires and the time interval for the burning.

Although a large amount of burning-rate data was obtained, the problems that resulted because of the poor reproducibility of some burning rates could not be entirely overcome. The principal causes of poor data were: premature burnout of the wires, which caused the clocks to stop too soon, and shorts between the insulated (hot) terminals and ground, which caused the clocks to run too long. The use of a formica sheet covering the terminal side of the strand holder, asbestos covering the hot terminals, and insulation around the lead wires greatly increased reliability. However, no satisfactory solution was found to the problem of preventing hot metal from occasionally severing a wire ahead of the burning surface. These problems are magnified by the large strands being burned and the large amounts of metal involved, both as powdered aluminum and the metal strips. Redesign of the strand holder would possibly alleviate this difficulty. In addition, better pressure control would be desirable–the present bleed valve permits variations of ±25 psi. As an alternative, the use of photographic techniques for determining the burning rates of these systems would provide interesting information concerning the topography of the burning surface.

For conventional propellant strands or strands containing low amounts of metal, good reliability is obtained. For example, good agreement with reported data was obtained for Aerojet Corp., Atlantic Research Corp., and B. F. Goodrich Co. propellants.

2.6 BURNING-RATE DATA

In the investigation of advanced concepts for high-energy propellants, the parameter of primary importance in both rocket design and future planning is the knowledge of burning characteristics. There are many variables affecting the burning of heterogeneous propellants, and no theory to date can reliably express these variables, except in specialized cases. In a case such as the one under investigation, the addition of a metal reinforcement further complicates this problem. It was the purpose of this

study to obtain, if possible, some idea of how the burning mechanism is affected by the incorporation of a structural element and how variations in this structure change the relative burning characteristics. The principal variables affecting burning rate are pressure, temperature, particle sizes, and fuel to oxidizer ratio. The equation used for relating burning rate and pressure is

$$r = ap^n \tag{2.1}$$

where r is the burning rate, p is pressure, and a and n (pressure exponent) are constants.

The difficulties in obtaining reproducible burning rates were noted previously; from 100 runs, only about 70 percent were satisfactory. Hence, only propellants with three metals at three thicknesses and essentially only one configuration were studied. All of the burning-rate data is tabulated in Appendix C for reference. The data plotted in Figs. 2-3, 2-4, 2-5, 2-6, and 2-7 are averaged values.

A summary of the burning-rate data for the propellants containing metal strips of different thicknesses is compared to the burning rate of the propellant without metal strips for both formulations (Table 2-1) in Figs. 2-4, 2-5, and 2-6. In the propellant with aluminum or brass, an expected increase in burning rate with the amount of metal is observed. Propellant with stainless steel, however, presents a different trend; here, added metal decreases burning rate. Of course, one would expect that a continued addition of metal to a propellant grain of given size would finally produce a maximum in the burning rate. This is evidently true with aluminum. The burning rates for 6-mil and 10-mil aluminum strips in strands (Formulation I) of the same overall dimensions approach the same values. The reason that an increased thickness of stainless steel decreases the burning rate is apparently because the maximum in this case has already been exceeded. It is also apparent from Figs. 2-4, 2-5, and 2-6 that real differences in slope [pressure exponent n of Eq. (2.1)] exist, but since the absolute values of the slope are as yet uncertain, a correlation was not made. A summary of the pressure exponents as derived from Figs. 2-4, 2-5, and 2-6 is given in Table 2-3.

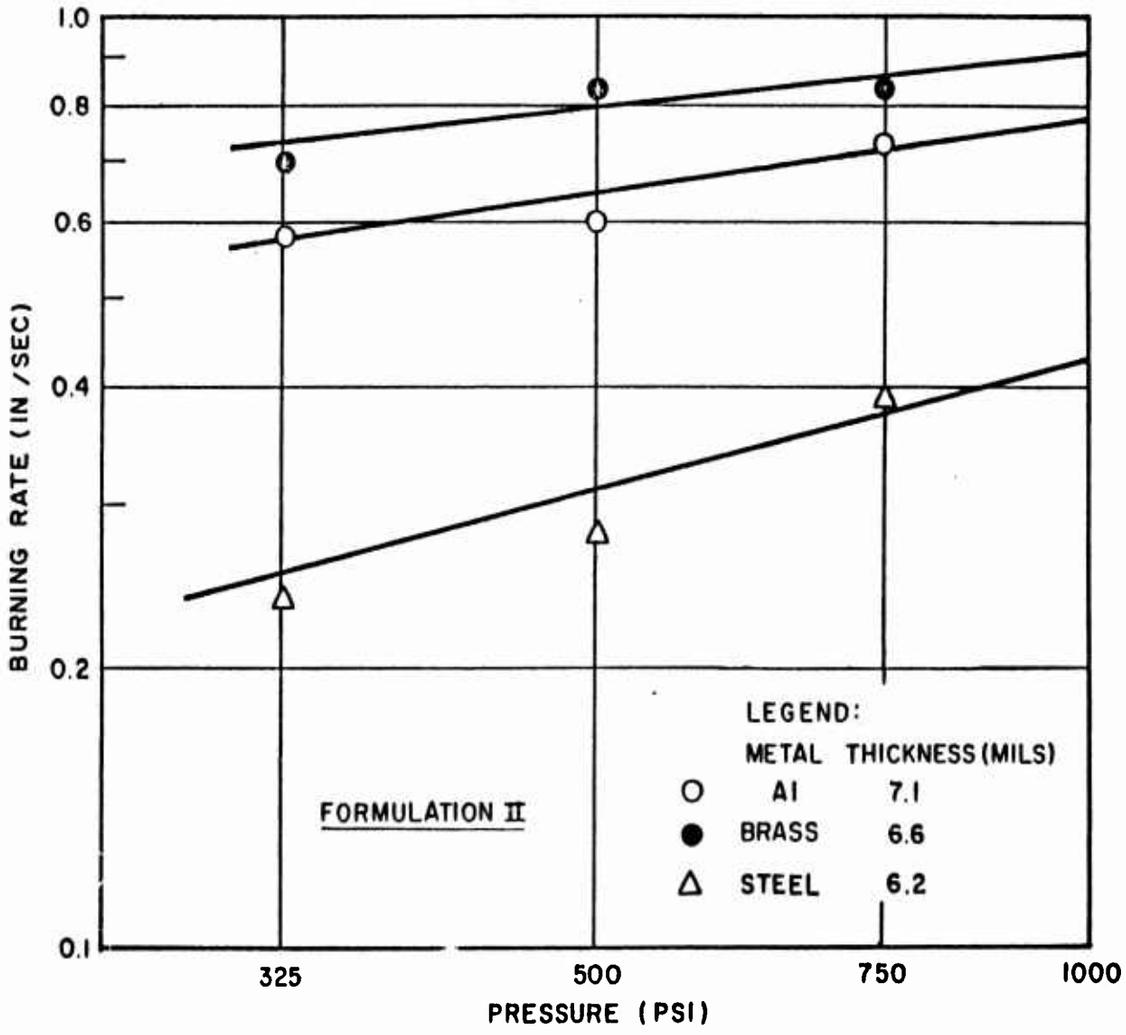

Fig. 2-3 Burning Rates as a Function of Pressure of Propellant Strands Containing Different Metal Strips

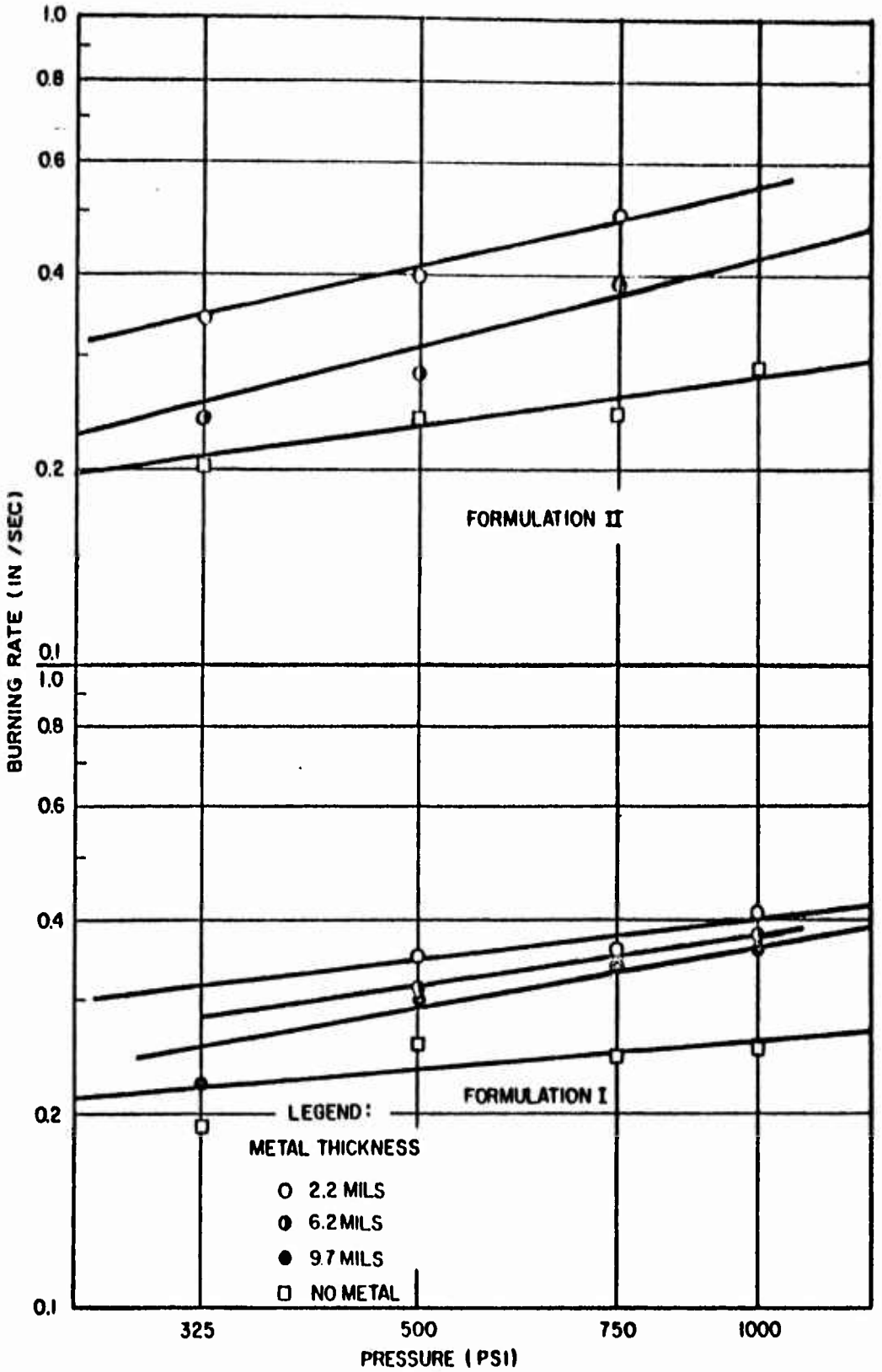

Fig. 2-4 Burning Rates as a Function of Pressure of Propellant Strands Containing Stainless-Steel Strips

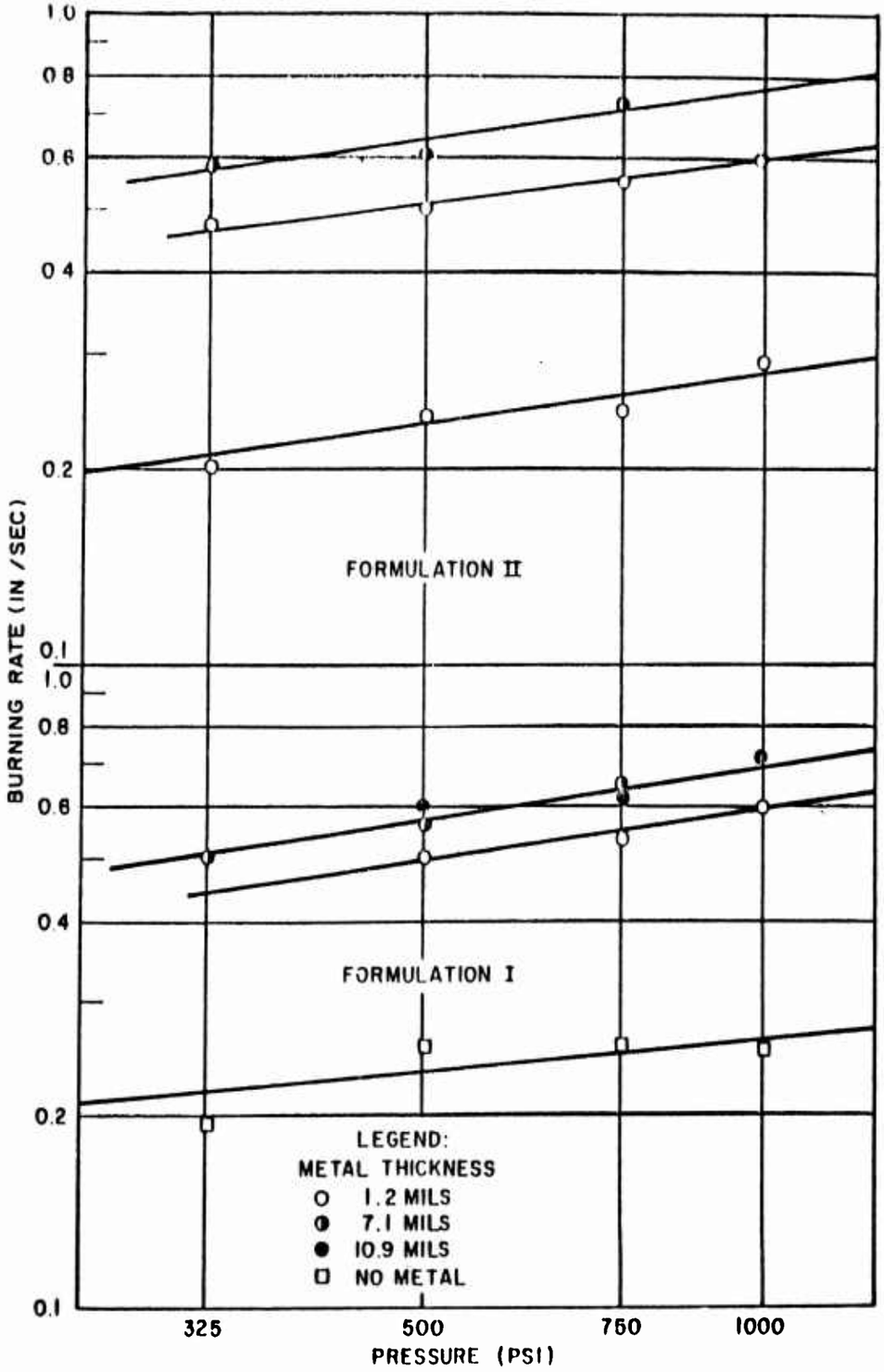

Fig. 2-5 Burning Rates as a Function of Pressure of Propellant Strands Containing Aluminum Strips

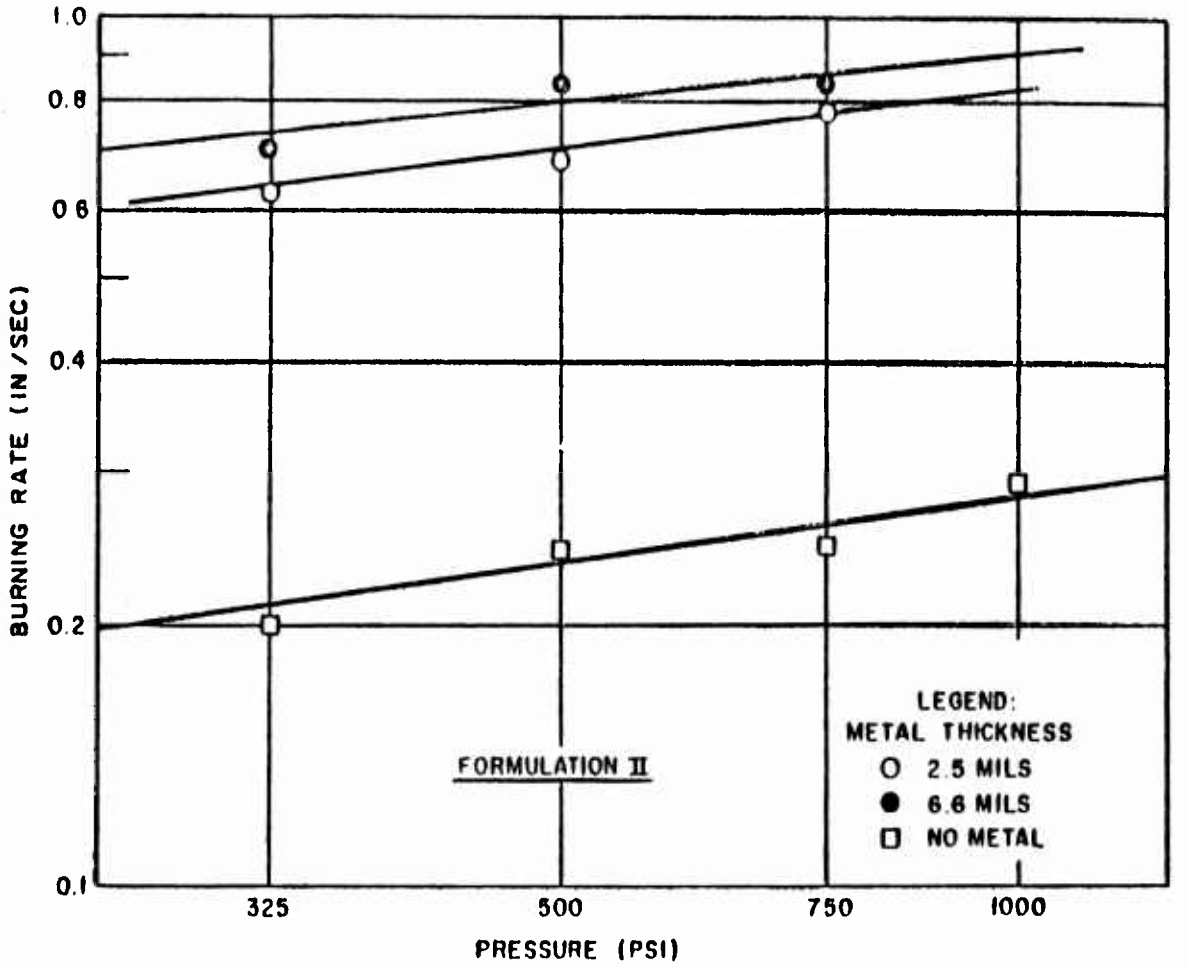

Fig. 2-6 Burning Rates as a Function of Pressure of Propellant Strands Containing Brass Strips

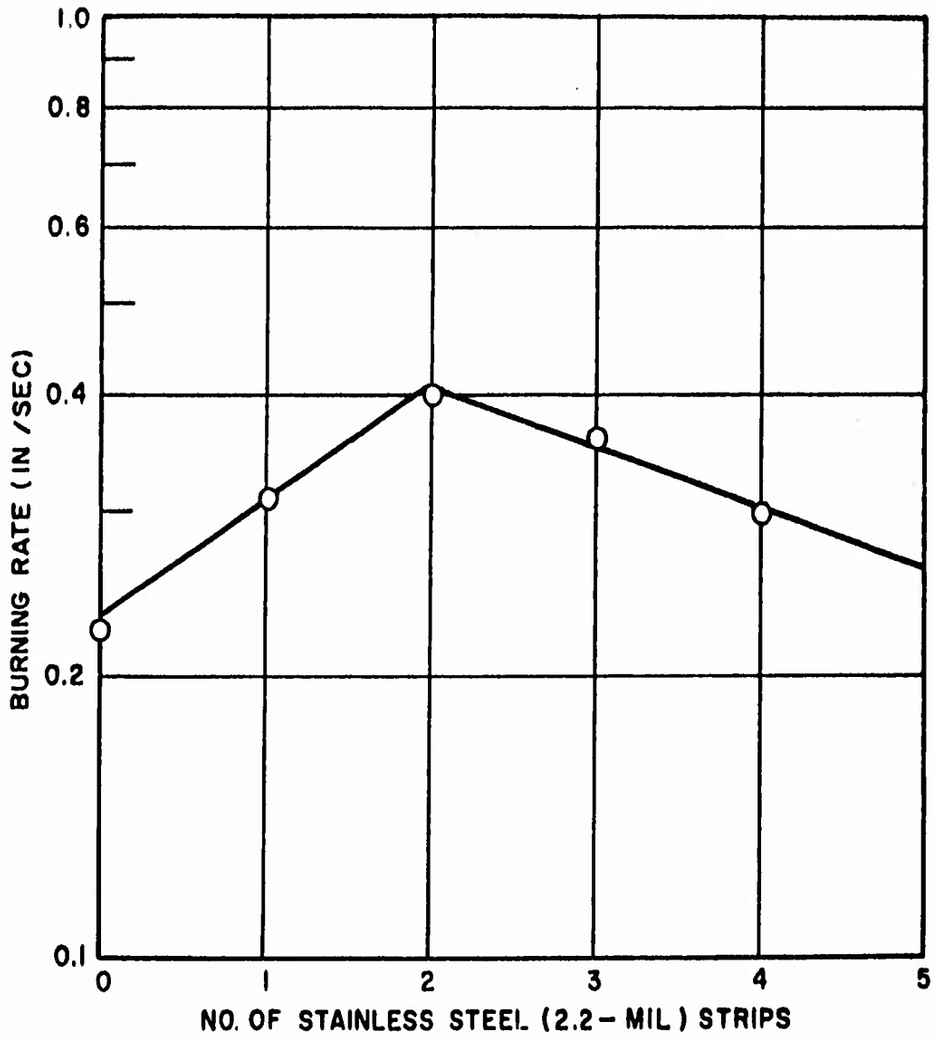

Fig. 2-7 Burning Rates at 325 psi of Propellant Strands Containing Stainless Steel (2.2 mil) as a Function of the Number of Strips

These results lead to the conclusion that strands containing several metal strips, if not too closely spaced and not too thick, would increase the burning rate. Also, that for a given strand, added strips of metal should cause the burning rate to maximize. This is clearly the case for steel at one pressure and one thickness (Table 2-4 and Fig. 2-7).

The incorporation of a metal strip in the direction of burning increases the linear burning rate normal to the end surface of the strand. This increase in burning rate is a function of the metal and is clearly shown in Fig. 2-3 for brass, aluminum, and stainless steel at comparable cross-sectional areas. The greater burning rate for brass, compared to aluminum and steel, is definite, and though some relation to thermal conductivity, specific heat, and phase change may exist, no simple explanation for the burning rate of brass over aluminum can be offered.

The preliminary theoretical treatment in Appendix A attempts to predict these phenomena. The resulting analysis, starting from a transient approach, predicts the effect of different-metal laminations on the burning rate as a function of the nondimensional parameter $R^* = hL/k_m$, the properties of the solid propellant, and the relative dimensions of the metal strip to propellant.

Appendix B discusses the topography of the burning surface and shows a relation be between the propagation rate down the longitudinal axis of the strand and the burning rate normal to the burning surface.

Table 2-3

PRESSURE EXPONENTS FOR PROPELLANT STRANDS CONTAINING DIFFERENT METAL STRIPS[a]

Metal	Thickness (mils)	Pressure Exponent	
		Formulation I	Formulation II
None	-	0.15	0.25
Brass	2.5	-	0.23
	6.6	-	0.19
Al	1.2	0.26	0.23
	7.1	0.26	0.26
	10.9	0.26	-
Stainless Steel	2.2	0.22	0.42
	6.2	0.27	0.46
	9.7	0.32	-

[a]Taken from Figs. 2-4, 2-5, and 2-6

Table 2-4

BURNING RATES OF PROPELLANT STRANDS CONTAINING STAINLESS STEEL (2.2 mil) AS A FUNCTION OF NUMBER OF STRIPS

No. of Strips	Burning Rate (in /sec)[a]
0	0.22[b]
1	0.31[b]
2	0.42
3	0.36
4	0.30

[a]At 325 psi

[b]From Fig. 2-4

Section 3

STRUCTURAL ASPECTS OF REINFORCING IN PROPELLANT GRAINS

3.1 INTRODUCTION

The behavior of grains containing various types of structural elements has not been studied previously. The purpose of this phase of the report is to analyze reinforcing problems and to determine the reinforcing value of structural elements in grains through experimental studies. Results of the studies are reported in this section.

3.2 BACKGROUND

A well-known application of reinforcing occurs in concrete structures. The Reinforcing is placed in regions of the structure subjected to tensile stress, because plain concrete has a strength in tension one-tenth to one-fifth of its strength in compression. By adding suitable steel reinforcing bars to the tension side of the beam, the load a simple beam of concrete can carry (including its own weight) is increased by a factor of 5 to 10. This factor will seem large compared to factors in examples discussed later. This is because the portion of concrete in tension (and which contains the reinforcing) is allowed to crack during the normal load-carrying function of the beam. (See Fig. 3-1.) "Hairline" cracks, as they are called, are barely, if at all, visible to the eye. Their presence does not indicate failure of the beam; but on the contrary, they show it is functioning as intended.

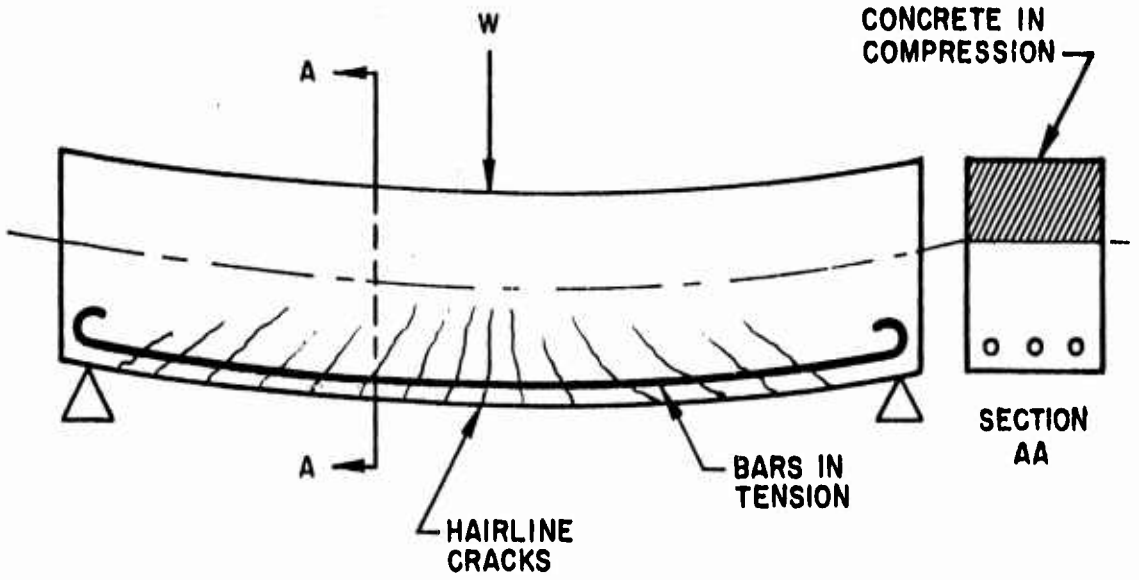

Fig. 3-1 Typical Behavior of a Reinforced Concrete Beam Subjected to Bending (Exaggerated)

As opposed to aluminum or some other metal, concrete is always reinforced with steel, partly because steel and concrete have approximately the same expansion coefficient. Were this not so, depending, of course, upon the degree of the discrepancy between the two materials, the reinforcing of concrete would not be feasible.

Concrete is a brittle material. Brittle materials, it is well known, are sensitive to discontinuities, irregularities, and inhomogeneities. That is to say, high stress concentrations that occur at such points when a load is applied are not relieved by local yielding. When a stress concentration reaches a certain level (under a gradually increasing load), local fracture occurs, and the stress concentration (followed by fracture) spreads until the result is total failure of the structure. Why can concrete, a brittle material, tolerate the presence of reinforcing steel, an inhomogenity, within itself? The pieces of steel are of the same general size and "roughness" as the stone aggregate that constitutes a large portion of the concrete. For any concrete, the level of stress called the "ultimate stress" is an average stress that includes a certain percentage of peak stress concentration points well above this average. Thus

the addition of reinforcing does not introduce a new (and larger) magnitude of irregularity or stress concentration. This is true of concrete that is reinforced even though it is under compressive stress, such as in columns; since in a sense, fracture occurs in the tension zone of a concrete beam but is prevented from spreading by the reinforcing.

Factors contributing to the successful application of reinforcing to concrete have been briefly reviewed. Hereafter, discussion of reinforcing will apply to propellant and the brittle plastics that have been used to simulate the propellant in preliminary testing.

Although it will severely limit the benefits to be obtained from reinforcing, it must be assumed, at this stage, that propellant material will not be allowed to crack in zones of tensile stress. This is assumed since reinforcing was proposed as a means of eliminating the cracking of propellant material under certain load conditions.

Another condition that must exist is the bonding of the reinforcing to the material it reinforces. With few exceptions (which are of no particular interest here), no benefit is to be derived from reinforcing which is not bonded, or at least "locked to" or "keyed into" the encasing material.

3.3 SYMBOLS

A	cross section area (in^2)
α	expansion coefficient ($in/in/^oF$)
B	reinforcing benefit (percent reduction in propellant stress caused by presence of reinforcing)
D	diameter of a circular cross section (in.)
d	depth of a cross section (in.)
δ	strain (change in length caused by stress, per unit length)
E	modulus of elasticity (psi)
f	stress (psi)
j	coefficient (in the expression for thermal stress – depends on stress distribution)
k	coefficient (in the expression for reinforcing benefit – depends on reinforcing configuration)
n	ratio E_r/E_p (elastic modulus of reinforcing divided by elastic modulus of propellant or plastic)
P	ratio A_r/A_p (area of reinforcing divided by the area of propellant or plastic, usually given as a percentage)
R	radius of a circular cross section (in.)
W	load on a structure, structural element, or specimen (lb)

Subscripts

p	designates "of propellant or plastic"
r	designates "of reinforcing"
u	designates "ultimate stress" (subscript to f)

The following basic relations are reviewed

$$\frac{W}{A} = f = E\delta \tag{3.1}$$

where W acts at the centroid of A .

3.4 REINFORCING CALCULATIONS

Consider a prismatic bar of propellant with several strands of reinforcing embedded in it so that the centroid of the propellant area coincides with the centroid of reinforcing. Assume this bar to be loaded axially (Fig. 3-2). If the reinforcing is bonded to the propellant, the strain in the reinforcing must be the same as the strain in the propellant, or

$$\delta_r = \delta_p \tag{3.2}$$

since

$$\delta_r = \frac{f_r}{E_r} \text{ and } \delta_p = \frac{f_p}{E_p}$$

$$\frac{f_r}{E_r} = \frac{f_p}{E_p} \text{ or } \frac{f_r}{f_p} = \frac{E_r}{E_p} = n \tag{3.3a}$$

If the reinforcing is steel with $E_r = 28 \times 10^6$ and the propellant has a modulus $E_p = 0.4 \times 10^6$, then $n = 70$; and since

$$f_r = nf_p \tag{3.3b}$$

it can be said that the stress in the reinforcing is always 70 times the stress in the propellant, provided the stress in either material does not exceed the proportional limit for that material.

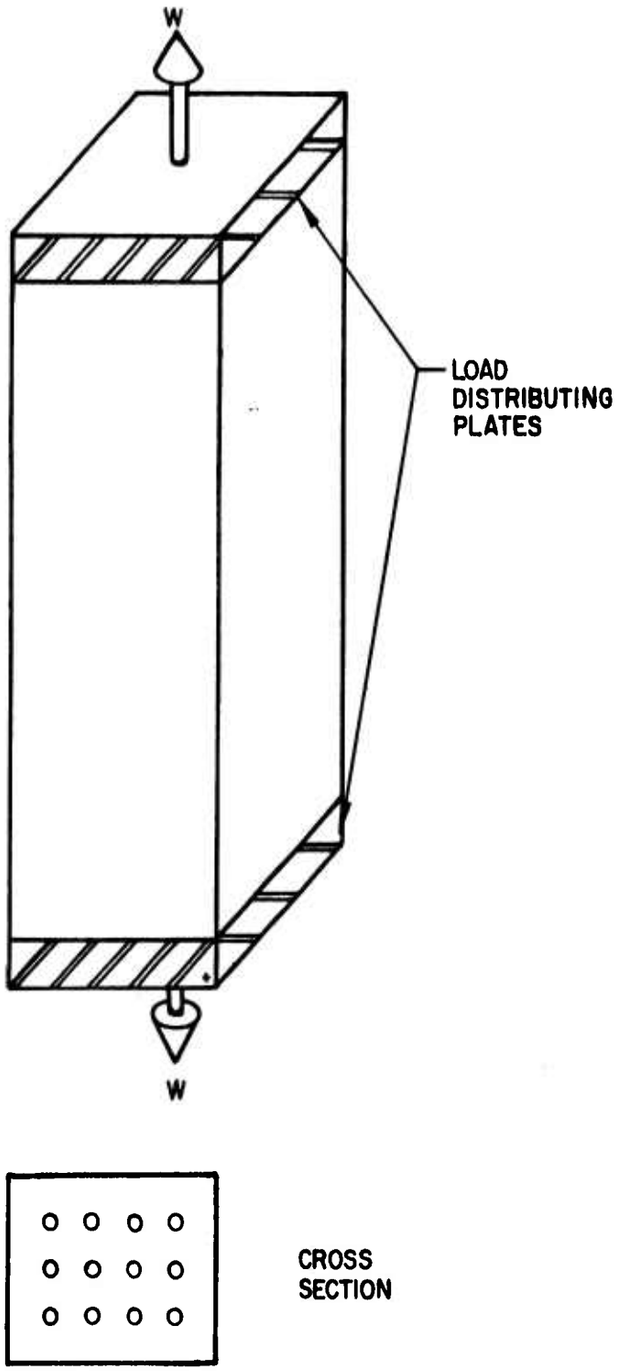

Fig. 3-2 Reinforced Propellant Bar Loaded Axially to Produce Uniform Tensile Stress

The relation between the total load W carried by the structural element shown in Fig. 3-2 and the stresses and areas of the component parts is

$$W = A_p f_p + A_r f_r \tag{3.4a}$$

This can be converted to

$$W = A_p f_p + A_r f_p n \tag{3.4b}$$

To be exact, the area of propellant that is replaced by the reinforcing must be deducted:

$$W = A_p f_p - A_r f_p + A_r f_p n \tag{3.5a}$$

Finally, this can be transformed to

$$W = f_p A_p \left[1 + (n-1)P\right] \tag{3.5b}$$

If the load W is held constant and f_p (the stress in the propellant) is to be studied for variations in P (the percentage of reinforcing), Eq. (3.5b) can be written in the form

$$f_p = \frac{W}{A_p \left[1 + (n-1)P\right]} \tag{3.5c}$$

If there is no reinforcing in the propellant P = 0 and $f_p = W/A_p$, and if we define the benefit B to be derived from the reinforcing as the percent reduction in propellant stress caused by the reinforcing, then

$$B = 100 \left[\frac{\left(\frac{W}{A_p}\right) - \left(\frac{W}{A_p}\right)\frac{1}{1 + (n-1)\frac{P}{100}}}{\left(\frac{W}{A_p}\right)} \right] \tag{3.6a}$$

or

$$B = 100 \left[1 - \frac{1}{1 + (n-1)\frac{P}{100}} \right] \qquad (3.6b)$$

where P and B are given in percentages.

Figure 3-3 shows curves of B versus P for different values of n ranging from n = 280 to n' = 40.4. (The prime notation acquires significance further in the report and can be overlooked at this stage.) This set of curves shows that the greatest benefit from reinforcing is obtained for the larger values of n. If the curves are all for stainless-steel reinforcing with $E_r = 28 \times 10^6$, we can get a 74 percent reduction in stress at 1 percent reinforcing if the elastic modulus of the propellant $E_p = 0.10 \times 10^6$; but when the propellant has $E_p = 0.50 \times 10^6$ the reduction in stress (B) is only 35 percent for 1 percent reinforcing. It is also evident that a 74-percent reduction in stress, achieved by 1-percent reinforcing can also mean that a specimen so reinforced will fail at approximately 4 times the axial load at which the unreinforced specimen will fail.

For a beam subjected to pure bending (Fig. 3-4), a similar set of benefit curves can be drawn. The derivation for B (the percent benefit) in pure bending, although elementary, is lengthy and will be omitted here. It can be shown that

$$B = 100 \left[1 - \frac{1}{1 + k(n-1)\frac{P}{100}} \right] \qquad (3.7a)$$

or

$$B = 100 \left[1 - \frac{1}{1 + (n'-1)\frac{P}{100}} \right] \qquad (3.7b)$$

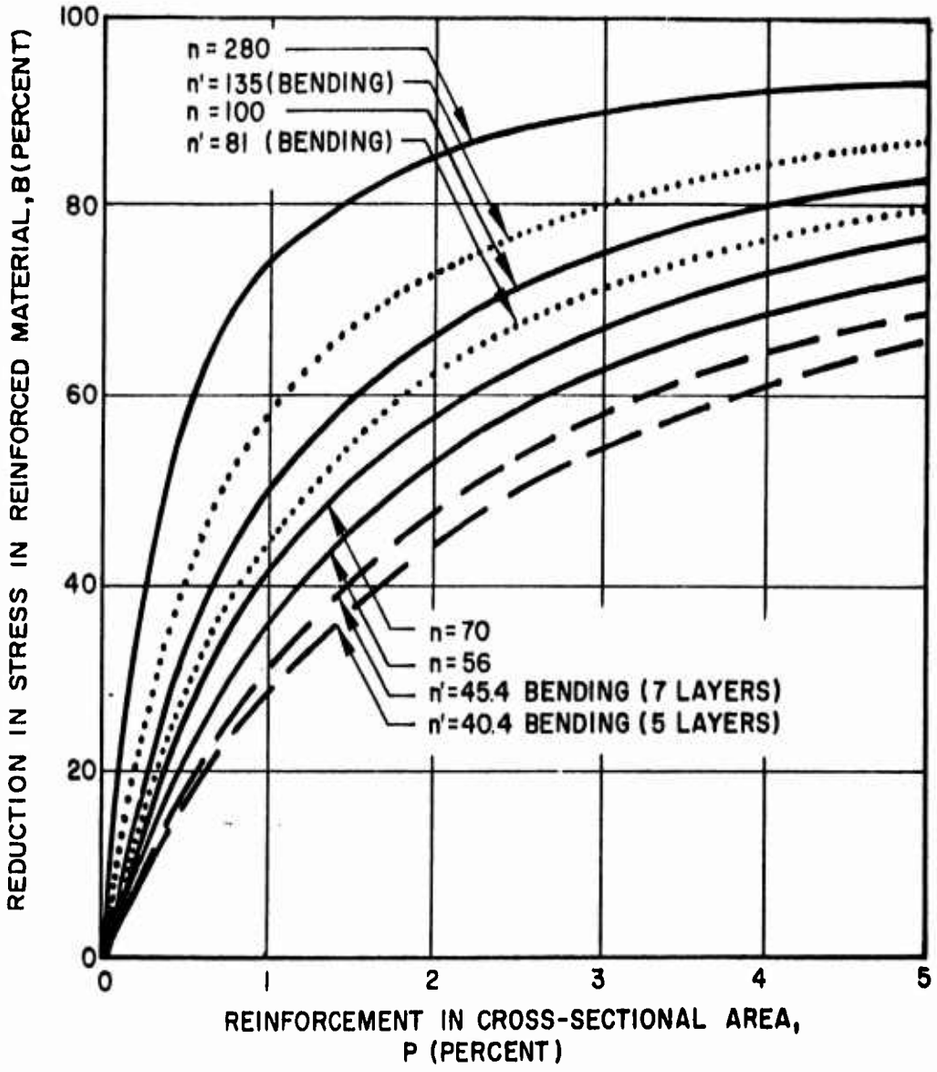

Fig. 3-3 Reinforcing Benefit Curves

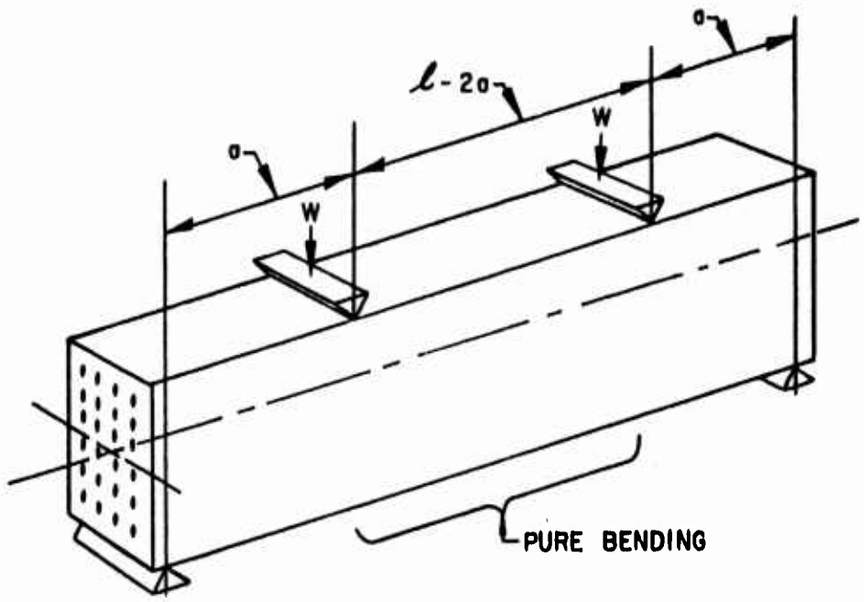

Fig. 3-4 Reinforced Beam Under Pure Bending

Eq. (3.6b) is the same as Eq. (3.7a) except for the introduction of the factor k, which is a function of the reinforcing arrangement.

If the reinforcing is equispaced in two mutually perpendicular directions throughout the beam's cross section, k is less than 1.0. As the spacing of reinforcing becomes smaller and smaller (for any constant value of P), k increases in value and approaches 1.0 as a limit. For equispaced reinforcing throughout the cross section of a beam in bending, however, k cannot exceed 1.0. In this event, the effect of k is to reduce the actual $n\left(\frac{E_r}{E_p}\right)$ to an "effective n', " thus

$$n' = k(n-1) + 1 \qquad (3.8)$$

Two beams with rectangular cross sections are shown in Figs. 3-5 and 3-6. The propellant meterial in both beams has an elastic modulus $E_p = 0.50 \times 10^6$ and the reinforcing in both is stainless steel with $E_r = 28 \times 10^6$, so that in both beams the actual $n = 56$. In Fig. 3-5, the reinforcing is arranged in five layers parallel to

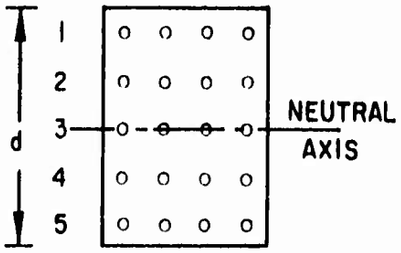

Fig. 3-5 Five-Layered Reinforcing (Cross Section)

the neutral axis, $k = 0.72$, $n' = 40.4$; and the benefit curve, so labeled, is shown as one of the dashed curves in Fig. 3-3. In Fig. 3-6, the reinforcing is arranged in seven layers (through the same depth d), and since the spacing is smaller, $k = 0.81$, $n' = 45.4$; and the benefit curve, labeled accordingly, is also shown as a dashed curve in Fig. 3-3.

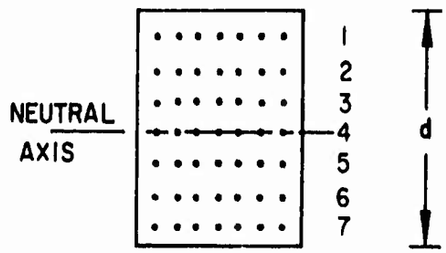

Fig. 3-6 Seven-Layered Reinforcing (Cross Section)

Thus far, it has been assumed that the reinforcing strands were equispaced in the two directions that are the rectangular axes of the cross section. This was for illustrative purposes only, since such an arrangement is inefficient for resisting bending stress.

In pure bending (Fig. 3-7), the stresses in a beam increase linearly from zero at the neutral axis. Thus, any reinforcing placed near the neutral axis is stressed only to a very low level. To obtain the maximum benefit from reinforcing in the

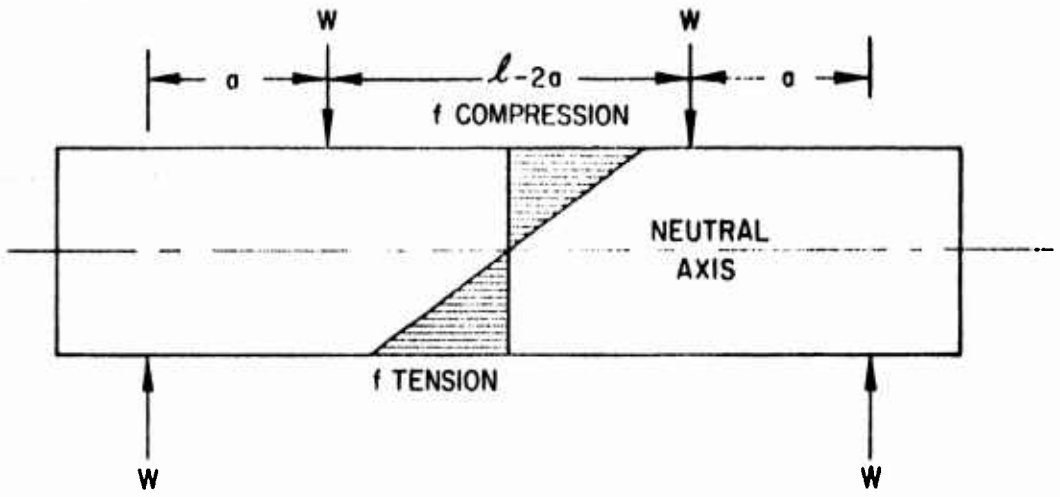

Fig. 3-7 Distribution of Stress Through Depth of a Beam in Pure Bending

event of bending, the reinforcing is placed as far from the neutral axis as possible, as shown in Fig. 3-8 where it is placed 9/20 of the beam depth from the neutral

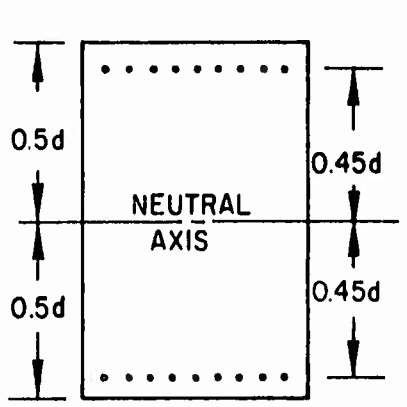

Fig. 3-8 Reinforcing Placed in Zones of High Stress (Cross Section)

axis. A certain amount of "cover" for the reinforcing must be allowed to assure good bonding of the reinforcing to the encasing material. With an efficient arrangement such as this one, $k = 2.43$, if $n = 56$ (as in the previous bending examples), then $n' = 135$. A dotted line in Fig. 3-3 is the resulting benefit curve.

For a beam with circular cross section and the reinforcing arranged in a circumferential layer at a radius of 0.45D (Fig. 3-9), n = 56, k = 1.46, and n' = 81. The corresponding benefit curve is shown in Fig. 3-3 by a dotted line. The addition of a second layer at a smaller radius would lower k and n' with a consequent lowering of the benefit curve. The placing of the reinforcement, clearly, is as important a factor as n.

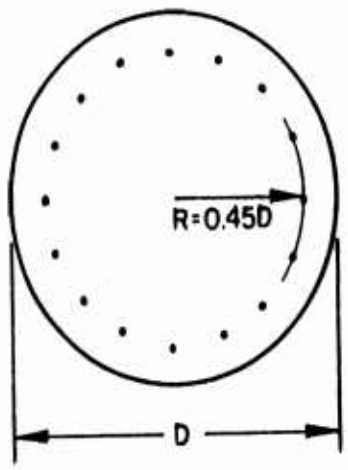

Fig. 3-9 Peripheral Reinforcing to Resist Bending About Any Diametral Axis

The above comments apply to beams symmetrically reinforced about the neutral axis. With such beams, k is a fairly simple function of the reinforcing placement. In beams unsymmetrically reinforced, k becomes a complicated function related not only to the placement of the reinforcing but also to n and P. In certain situations, especially where stress concentration effects are included (discussed later), k becomes impossible to compute or predict approximately and has to be determined experimentally. For unsymmetrical reinforcing of a simple configuration free of stress concentration, k will range between 1.0 and 2.5, according to estimates.

3.5 REINFORCING AT POINTS OF STRESS CONCENTRATION AND IN THICK-WALLED PRESSURE CYLINDERS

In a thick-walled cylinder subjected to internal pressure, as in a propellant grain with a cylindrical cavity, the circumferential stress is tensile and varies across the radial thickness (Fig. 3-10). Depending upon the proportions, the circumferential

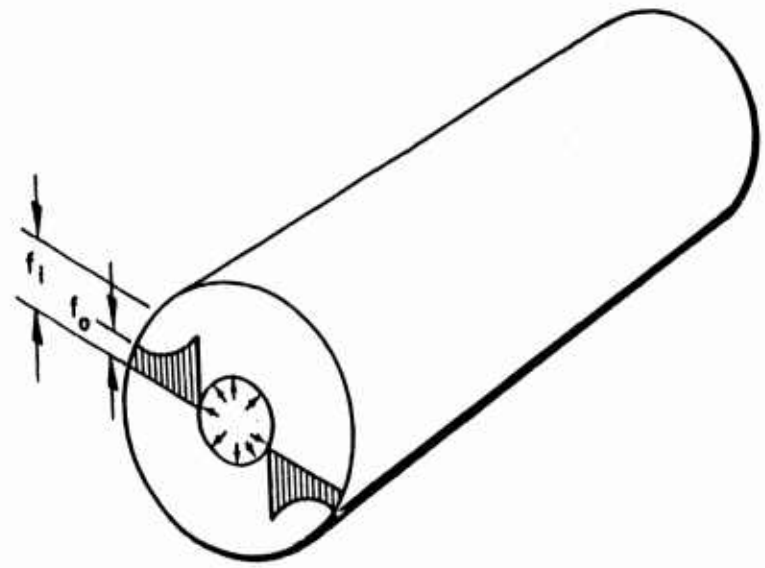

Fig. 3-10 Distribution of Circumferential Tensile Stress in a Thick-Walled Cylinder Under Internal Pressure

stress at the inner face can be as much as, or more than, twice the circumferential stress at the outer face. When this is true, equispacing of circumferential reinforcing throughout the thickness is inefficient for the same reason as in pure bending (i.e., many strands are not located where they will do the most good).

The addition of too many strands at the inner edge, where they would at first appear to do the most good, might cause a large shift of the circumferential stress centroid toward the center, bringing about a condition of diminishing returns. Since the

location of this centroid (for an elaborate reinforcing pattern) and the derivation of an equation for B (the reinforcing benefit) are no longer a simple matter – perhaps not even possible by analytical methods – they are best determined experimentally on a model by some technique such as photoelasticity or Photostress. It is estimated, and some tests have already tended to substantiate the estimate, that k will be less than unity or not very much larger than unity even under the most favorable (experimentally determined) layout of reinforcing. In other words, using the actual n will give a fair estimate of the benefit to be expected, and the curves of Fig. 3-3 will give any specific value of n.

If the propellant grain has a cavity other than circular (in cross section), any deviation from the circle can be considered as acting like a notch (of large radius in some cases) cut into a thick-walled cylinder (Fig. 3-11).

The effect is a "stress concentration." The circumferential stress at the inner-edge will be greater by an even larger factor than outer-edge stress. Portions of the propellant that extend radially inward from the thick wall can be considered structurally nonexistent and merely as dangling appendages; but in this sense, they are still likely to break off if the material is brittle and the unit subjected to large shocks.

In such a configuration, an expression for B can not be determined by theoretical methods, but its curve can be plotted from experimental data based on a series of tests of different models.

The factor k, it should be pointed out, exists only when stress distribution is nonuniform; a nonuniform distribution as shown in Fig. 3-11 is equivalent to a bending stress superimposed on a uniform stress. This comparison is illustrated in Fig. 3-12. Thus, a nonuniform stress, whether caused by curvature or stress concentration, produces conditions requiring the factor k. Furthermore, if the centroid of reinforcing does not coincide with the centroid of uniform stress, this too causes

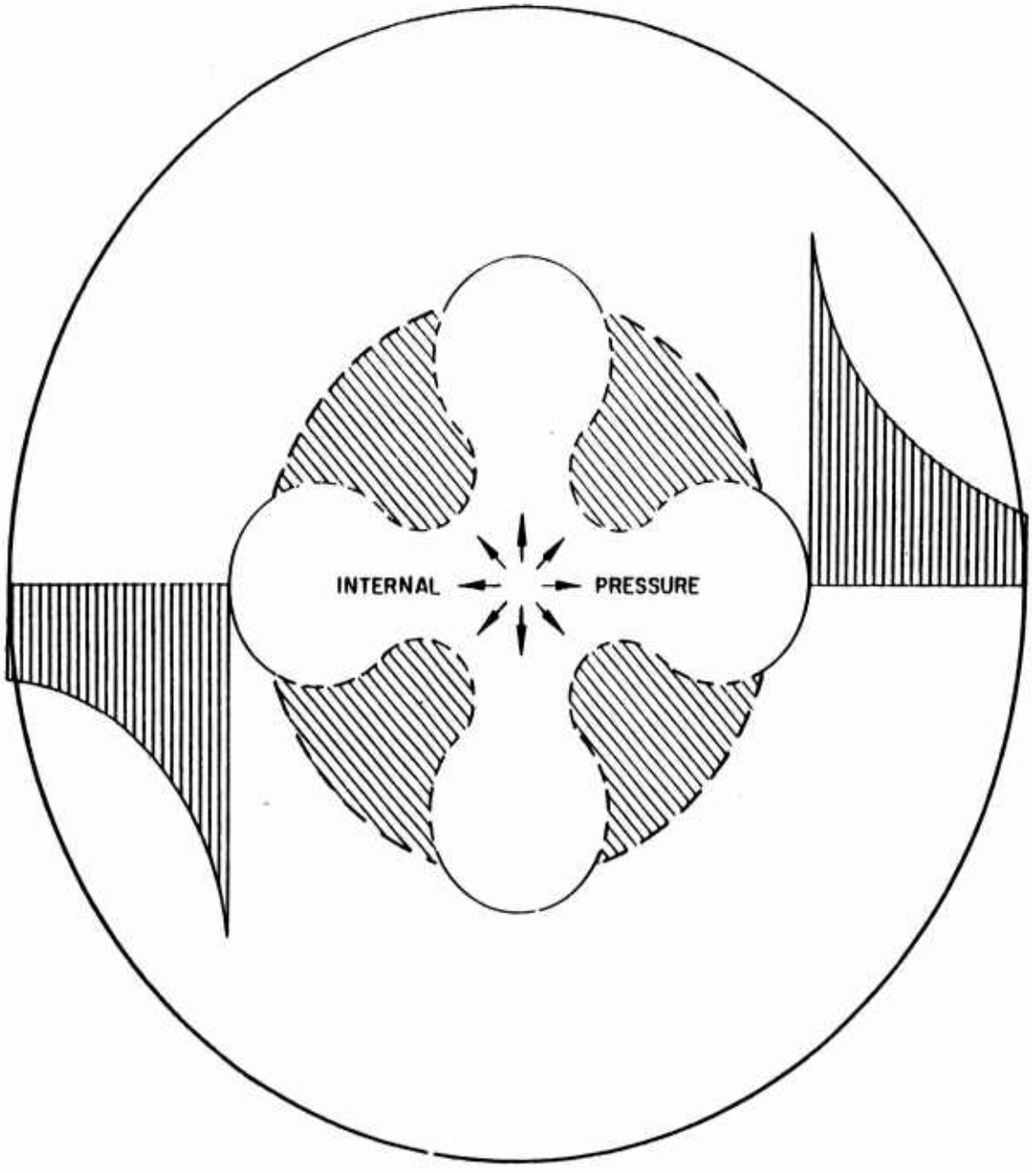

Fig. 3-11 Distribution of Circumferential (Tensile) Stress for a Propellant With Cloverleaf Cavity

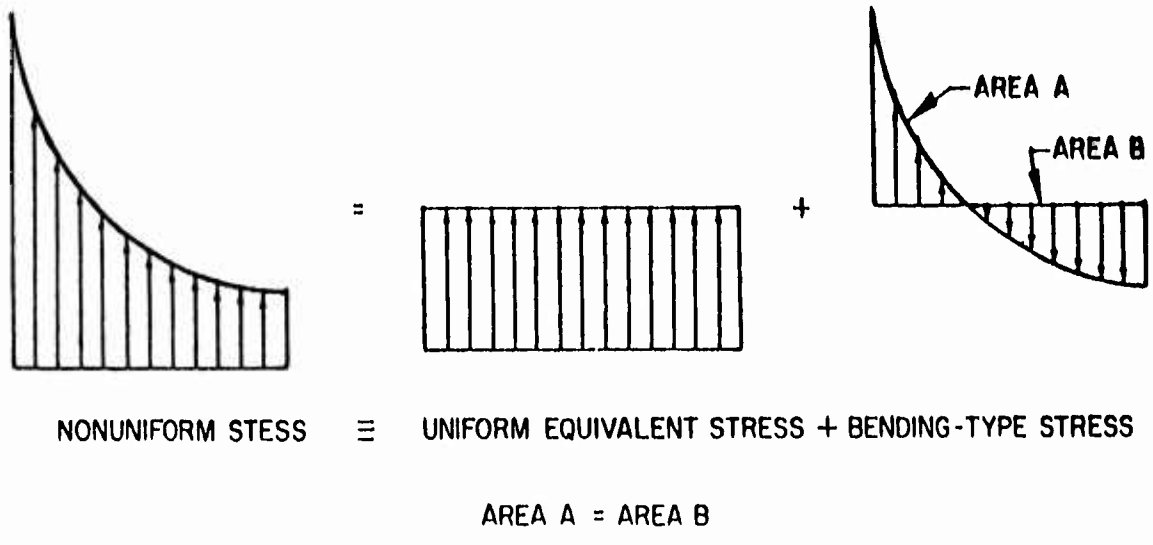

Fig. 3-12 Nonuniform Stress Equivalent to a Uniform Equivalent Stress Plus a Bending-Type Stress

bending, and k must also be introduced. Only where the reinforcing centroid coincides with the centroid of a uniform stress does $k = 1.0$ and in such cases it is omitted from the equation for B. [See Eq. (3.6b).]

To recapitulate this discussion of reinforcing, k is unity for uniformly-stressed and uniformly-reinforced cross sections. If nonuniform stress is introduced (and uniform reinforcing retained), k becomes less than unity. To increase the value of k above unity in nonuniform stress, reinforcing must be placed only in the regions of higher stress. There is an optimum position and percentage of reinforcing in cases of nonuniform stress. Beyond this optimum, values of k start decreasing again. A stress concentration can be regarded as a nonuniform stress condition of an extreme nature. The greater the stress concentration, the lower the optimum value of k is likely to be. In fact, in extreme cases, a stress concentration is likely to prevent k from exceeding unity even under the most favorable reinforcing placement.

Thus, the important factors in reinforcing design are the percentage P, the ratio of the elastic moduli n, the specific placing of the reinforcing, and the avoidance of stress concentration.

3.6 REINFORCING AS A SOURCE OF STRESS CONCENTRATION

As explained in subsection 3.2 on reinforcing of concrete, the reinforcing itself could be a source of stress concentration in that it constitutes a discontinuity or inhomogeneity in the reinforced material. The particles or granules in the propellant may have a maximum diameter of 1/100 in. If they are sharp and needle-like, their stress-causing potential is magnified, and their effective size is greater than their true size. In any case, the ultimate tensile stress is a statistical average influenced by this effective size of the particles. Rough reinforcing wire of a diameter considerably greater than the effective grain size could initiate a stress-concentration failure. In several laboratory tests, a wire terminating abruptly in a region of stress caused tensile specimens to fail at 20 to 30 percent of their usual ultimate tensile strength. Each failure was at the termination of the wire. When the reinforcing wire was extended to a region of lowered stress, the failures did not occur (Fig. 3-13).

Similar failures occurred in models of circular cross-sectioned propellant grains. To avoid this type of failure, which undermines the purpose of the reinforcing, reinforcing strand sizes may have to be limited, and reinforcing wires will have to be smooth, clean, and terminated and spliced in regions of low stress.

3.7 EXPANSION COEFFICIENTS OF REINFORCING AND REINFORCED MATERIALS

If the expansion coefficient of the propellant is larger than the expansion coefficient of the reinforcing, tensile stresses which tend to crack the propellant will occur if the reinforced propellant experiences a drop in temperature. For the simple case of a beam in which the centroid of the reinforcing coincides with the centroid of the propellant material, the maximum tensile stress in the propellant will be uniform and axial and is given by

$$f_p(\max) = -\frac{2nPE_p(\alpha_p-\alpha_r)(\Delta T)}{100 + nP} \qquad (3.9)$$

where ΔT is the temperature change.

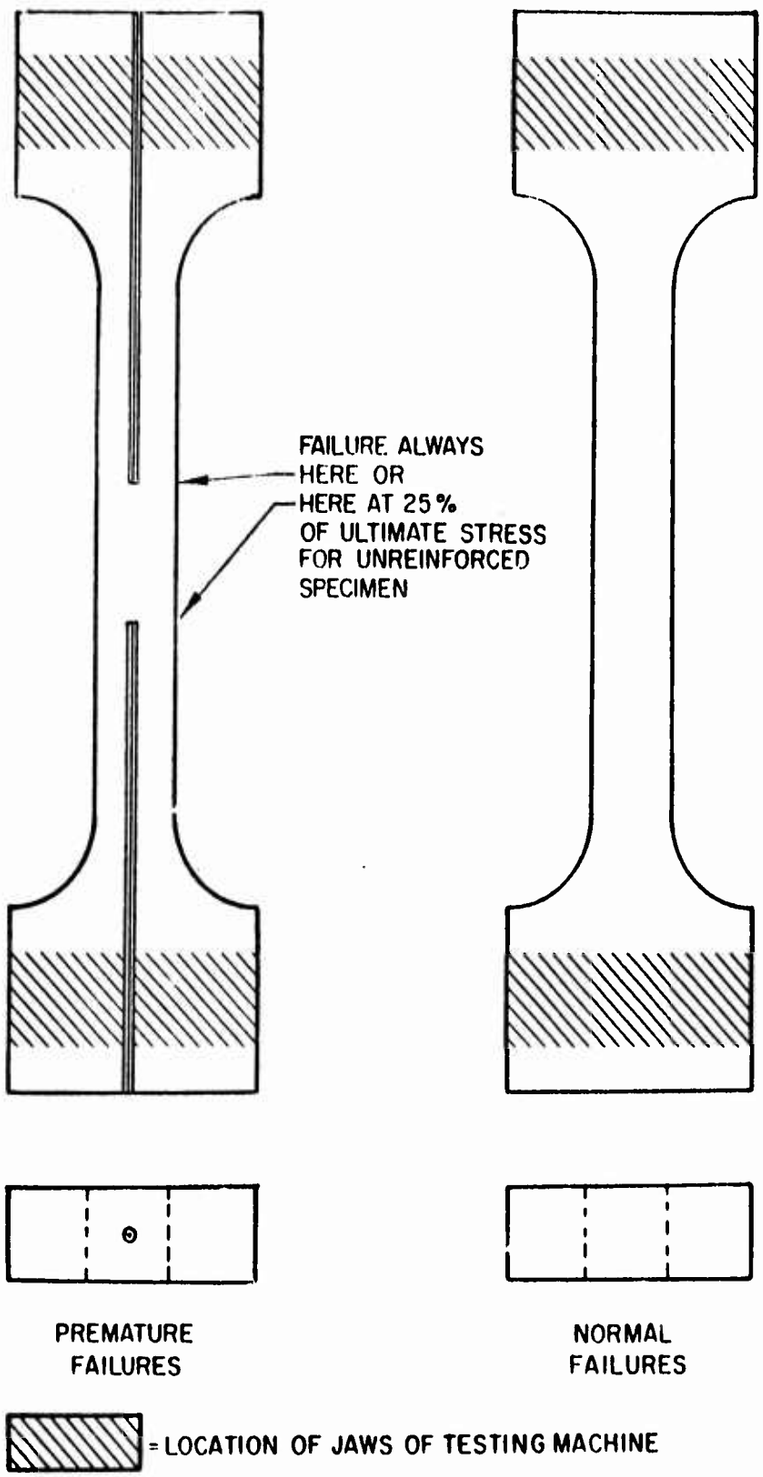

Fig. 3-13 Dumbbell Specimens for Reinforcing Discontinuity Tests

For illustration, let it be assumed that $n = 70$, $E_p = 0.5 \times 10^6$, $P = 1.5$ (%), $\alpha_p = 50 \times 10^{-6}$, $\alpha_r = 7 \times 10^{-6}$, and that the propellant fails under a tensile stress of 2000 psi. To determine the temperature drop that will cause cracking of the propellant, set $f_p = 2000$ and

$$2000 = - \frac{2 \times 70 \times 1.5 \times (0.5 \times 10^6)(50-7)\,10^{-6} \times (\Delta T)}{100 + 70 \times 1.5}$$

from which $\Delta T = -91°F$ (the minus sign indicates a temperature drop).

No study has been made of the surface (shear) stress at which the bond between reinforcing and propellant will be destroyed, but it is assumed in the above example that the bond was good and that failure of the specimen did not occur because of delamination of the reinforcing before tensile failure of the propellant.

Where the reinforcing consists of a few large strands instead of many small ones (resulting in low surface area per unit volume, i.e., low peripheral length per unit cross-sectional area), failure through delamination could conceivably occur for a smaller temperature drop than the 90°F calculated above.

Furthermore, the calculation was for coincident centroids of the two materials, an arrangement that is unlikely since it has been shown that concentrations of reinforcing inzones of higher stress are more efficient. If the centroids are not coincident, the thermal stress will be greater than for the case of coincident centroids, and the multiplication factor for this can be as large as three.

If the reinforcing is in a zone of stress concentration, the thermal stresses (as calculated by the simplified equation above) will be increased in approximately the same proportion as the stress concentration represents an increase over the "calculated uniform equivalent stress." (See Fig. 3-12.) In other words, if the "stress concentration factor" (a rather vague concept) is two, it would take half as much of a temperature

drop to produce tensile failure of the propellant, namely 45.5°F for the combination of materials in the example above.

For cylinders reinforced in the circumferential direction, circumferential thermal stress in the propellant is given by

$$f_p = - \frac{jnPE_p (\alpha_p - \alpha_r)(\Delta T)}{100 + nP} \qquad (3.10)$$

where j is some constant for any specific configuration of reinforcing and specific cavity cross section. It is known that j is unity for a thin-walled cylinder and that values of j increase as the wall increases in thickness and as stress concentrations are introduced. It is not difficult to visualize a case where j would have the value of five.

To avoid undermining the benefit from reinforcing by the thermal behavior of the materials, as evident from Eqs. (3.9) and (3.10) for thermal stress, the difference between the expansion coefficients $(\alpha_p - \alpha_r)$ will have to be held as small as possible. A low elastic modulus for the propellant (E_p) will also improve matters in this respect.

3.8 OTHER CONSIDERATIONS

If efforts are made to increase the value of n for a combination of materials, and if this is done by a composition that lowers the elastic modulus of the propellant (E_p), it is possible that the ultimate tensile strength will also be lowered. In concrete, for instance, the ratio $E_c/f_{cu} = 1000$, where the subscript c refers to concrete and u to ultimate stress. For a propellant, the ratio would equal some other constant (such as 40), or it may vary nonlinearly. But it is almost certain that a decrease in modulus will cause a decrease in strength for any one type of material. Thus in this respect, there is also an optimum that has to be determined experimentally.

If the reinforcing is steel, with a pronounced yield point, the design of the reinforcing could employ the strength of the reinforcing above the yield point. This involves new factors which have not been discussed. The most important of these is percent elongation (strain) that the propellant will tolerate just before tensile failure.

Another problem may be the placing of reinforcing after a specific percentage has been determined as desirable, especially where k is more than unity, thereby indicating a concentration of reinforcement. In reinforced concrete, general practice dictates that there be a minimum clear space between bars equal to three bar diameters. With a finer-grained material, this could be reduced to two bar diameters. But intuition tells us that less than this might cause "honeycombing" (air voids) if the propellant "poured" is anything more viscous than water.

To illustrate how restrictive this minimum of two bar diameters can be, let us suppose that design curves indicated that reinforcing for bending about any axis of a circular cross section 12 in. in diameter should be 2 percent. Let us also assume that the reinforcing had to be 1/8-in.-diameter wires spaced on a circumference located at 0.45D. (See Fig. 3-9.)

The cross-sectional area of a 12-in.-diameter propellant is 113 in^2; 2 percent of this is 2.26 in^2 of reinforcing. The cross-sectional area of wire 1/8 in. in diameter is 0.0123 in^2. This means that 184 wires are needed (2.26 ÷ 0.0123). The circumference at (0.45D) radius is 34 in. The center-to-center spacing of the 184 1/8-in. wires would then have to 0.185 in. (34 ÷ 184). But the two-bar diameter rule calls for 0.375-in. spacing (center-to-center). The bars would therefore have to be arranged in two circles. This would reduce k, which probably means that P would have to be increased, which means more bars, which means more circles, etc.

The difficulty might be relieved by trying 1/4-in. bars. Since they have four times as much area, only 46 would be needed to supply the required 2 percent. The center-to-center spacing would be 0.74 in. (34 ÷ 36), and since the two-bar diameter rule calls

for a minimum spacing of 0.75 in., the small shortcoming might be overlooked. However, the larger bars might fail in bond, or they might be large enough to cause stress concentrations.

Where bars are concentrated, the value of P can be misleading, and it may be desirable in further studies to redefine P so that it is more representative in the locale where the reinforcing is concentrated.

Shear stress may be a cause of failure, and in this event, reinforcing is likely to be helpful. But calculations for and predictions on shear reinforcing are not possible unless very specific information is available on shape and size of structure, properties, properties of the materials, and the cause of the shear stress.

3.9 STRUCTURAL TESTS

Structural tests were performed to determine the validity of the methods of calculation presented in subsection 3.4 and to evaluate the benefit B and the k factor in configurations where calculations are not possible. Some of the tests were performed to establish properties of one propellant and of an epoxy resin used to simulate the propellant in reinforced models. Table 3-1 shows that the comparison between the properties of the epoxy resin and the propellant composition is not as favorable as could be hoped for.

Table 3-1

PHYSICAL PROPERTIES OF MATERIALS

	Epoxy Resin (Average)	Propellant Composition Formulation I*
E_p	0.4×10^6 psi	0.08×10^6 psi
$f_{tensile\ ultimate}$	10.000 psi	2.000 psi
$\delta_{ultimate}$	3.5%	1.8%
α	50×10^{-6} in /in /^oF	Unknown

*See Table 2-1

Nevertheless, tests have served the useful purpose of showing that (within the proportional limits of the materials) the reinforcing benefit, as measured experimentally, agreed closely with theoretical predictions based on the equations given in subsection 3.4.

In reinforced dumbbell speciments (Fig. 3-14) loaded to produce uniform axial stress, the predicted strain δ_p over a 2-in. gage length (calculated using the theoretical equations matched the measured strain δ_p to an average accuracy of 3 percent for 10 specimens. The reinforcing used was stainless-steel wire: E_r was 28×10^6; values of P ranged from 5 to 10 percent; and E_p was 0.4×10^6, giving $n = 70$.

Tests were also performed on a simulated propellant grain cross section. The cavity cross section was a four-pointed "rounded" star (Fig. 3-15). Tests were run on three models. Model No. 1 was not reinforced. Model No. 2 was reinforced with No. 30 wire mesh arranged in a spiral (Fig. 3-16). Model No. 3 was reinforced on one side with a single 1/16-in.-diameter stainless-steel wire located 1/8 in. from the inner surface at one of the radial sections of maximum stress; the diametrically opposite radial section of Model No. 3 was reinforced with two 1/16-in.-diameter wires also located 1/8 in. from the inner edge (Fig. 3-17).

Stress distribution was studied at radial sections where the radial thickness is least (section A-A, Figs. 3-16, 3-17, and 3-18). At these points, the cross-sectional area of plastic $A_p = 0.47\ in^2$. The area of six circumferential strands of the wire mesh was $A_r = 0.00254\ in^2$, so that P_2 (for Model No. 2) was 0.54 percent. In Model No. 3, the area of the single wire was $0.0031\ in^2$, so that P_3 (Model No. 3, single-wire side) = 0.67 percent, and P_4 (Model No. 3, two-wire side) = 1.33 percent.

The same diametrical tensile load was applied to the three models (Fig. 3-18), and measurements (or photographs) were then taken at sections such as A-A in Fig. 3-18.

Under this loading condition, the circumferential stress across any section A-A is a bending stress (Fig. 3-19) with f_i, the stress at the inner edge, being tension and

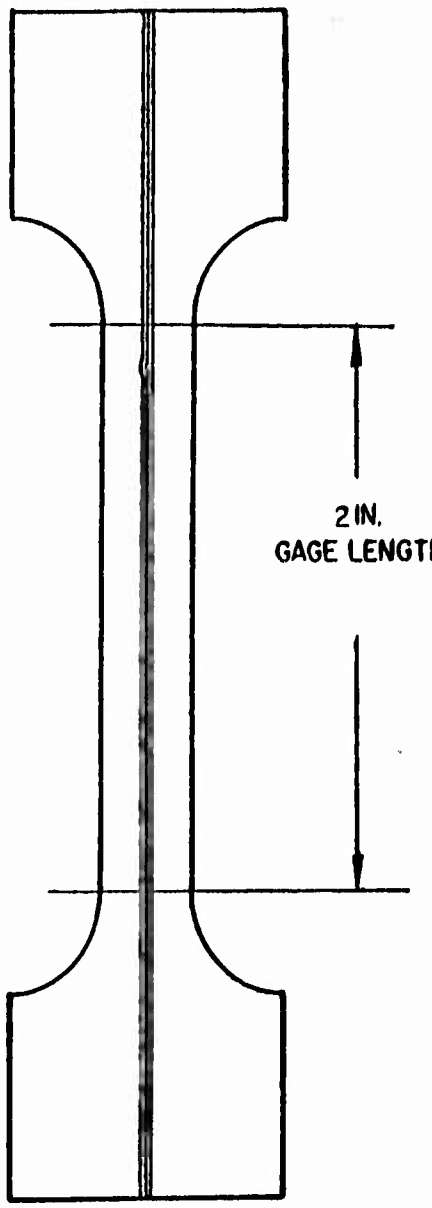

Fig. 3-14 Typical Reinforced Epoxy Dumbbell Specimen

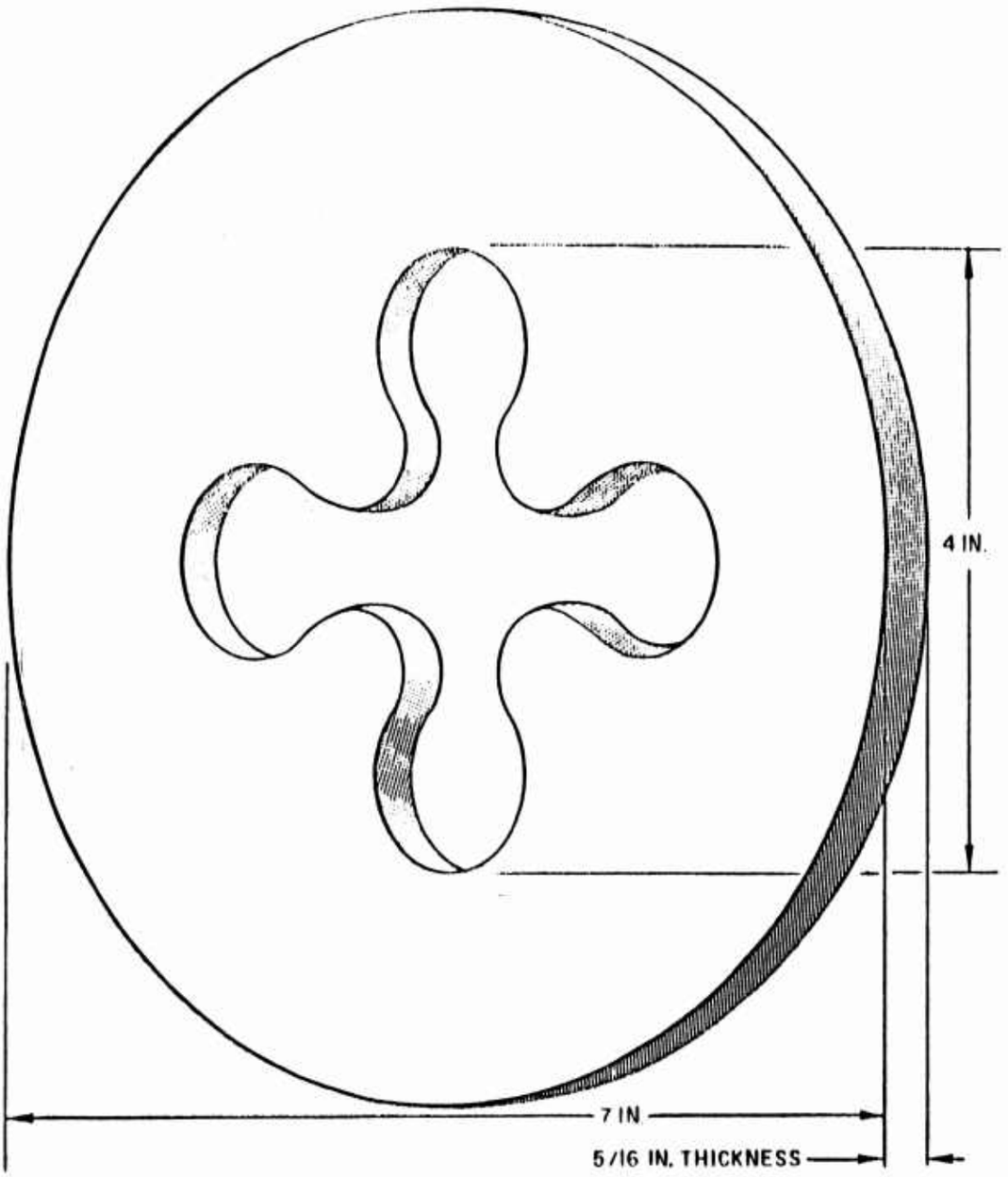

Fig. 3-15 Simulated Propellant Grain Cross Section (Model No. 1)

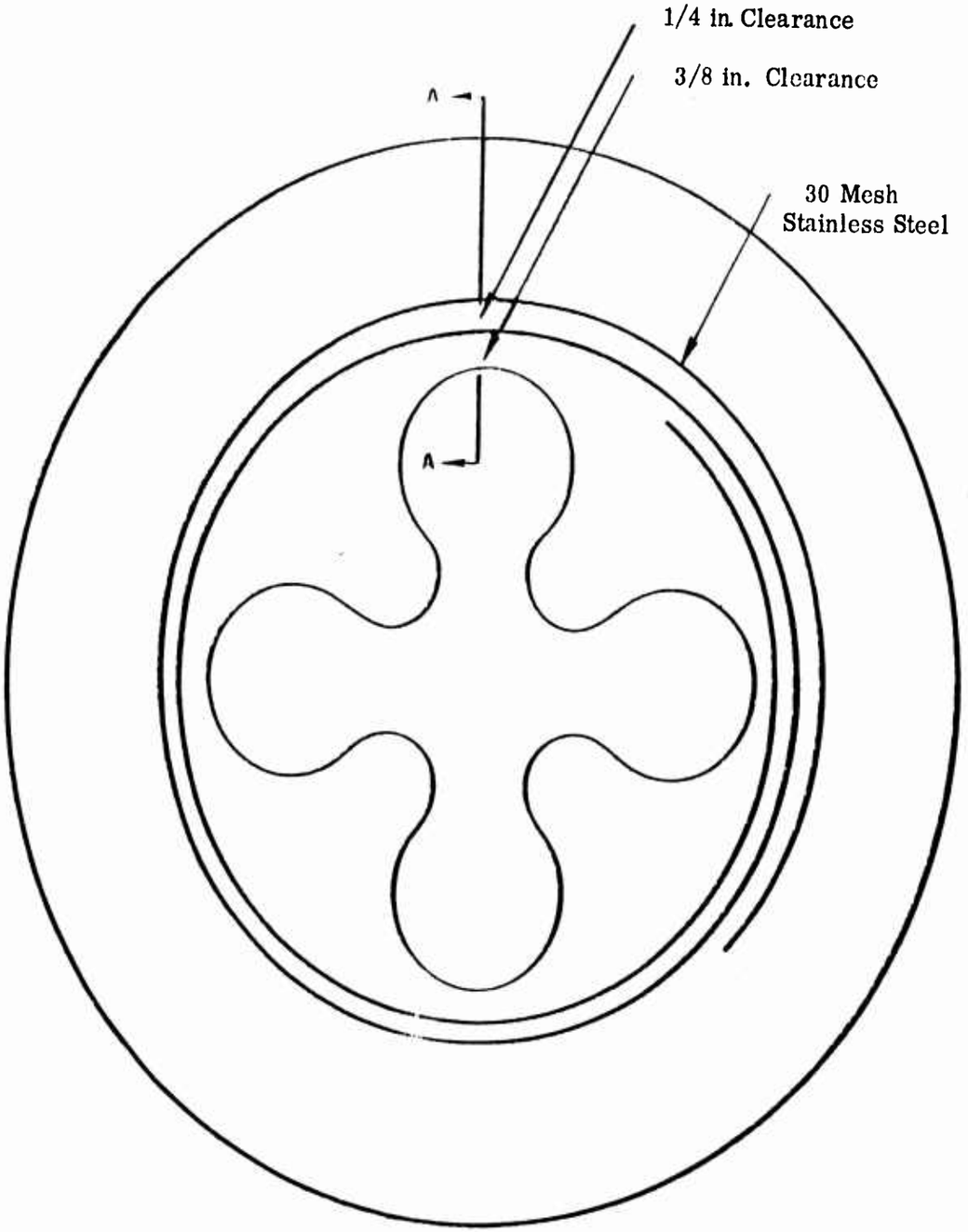

Fig. 3-16 Wire Mesh Reinforced (Model No. 2)

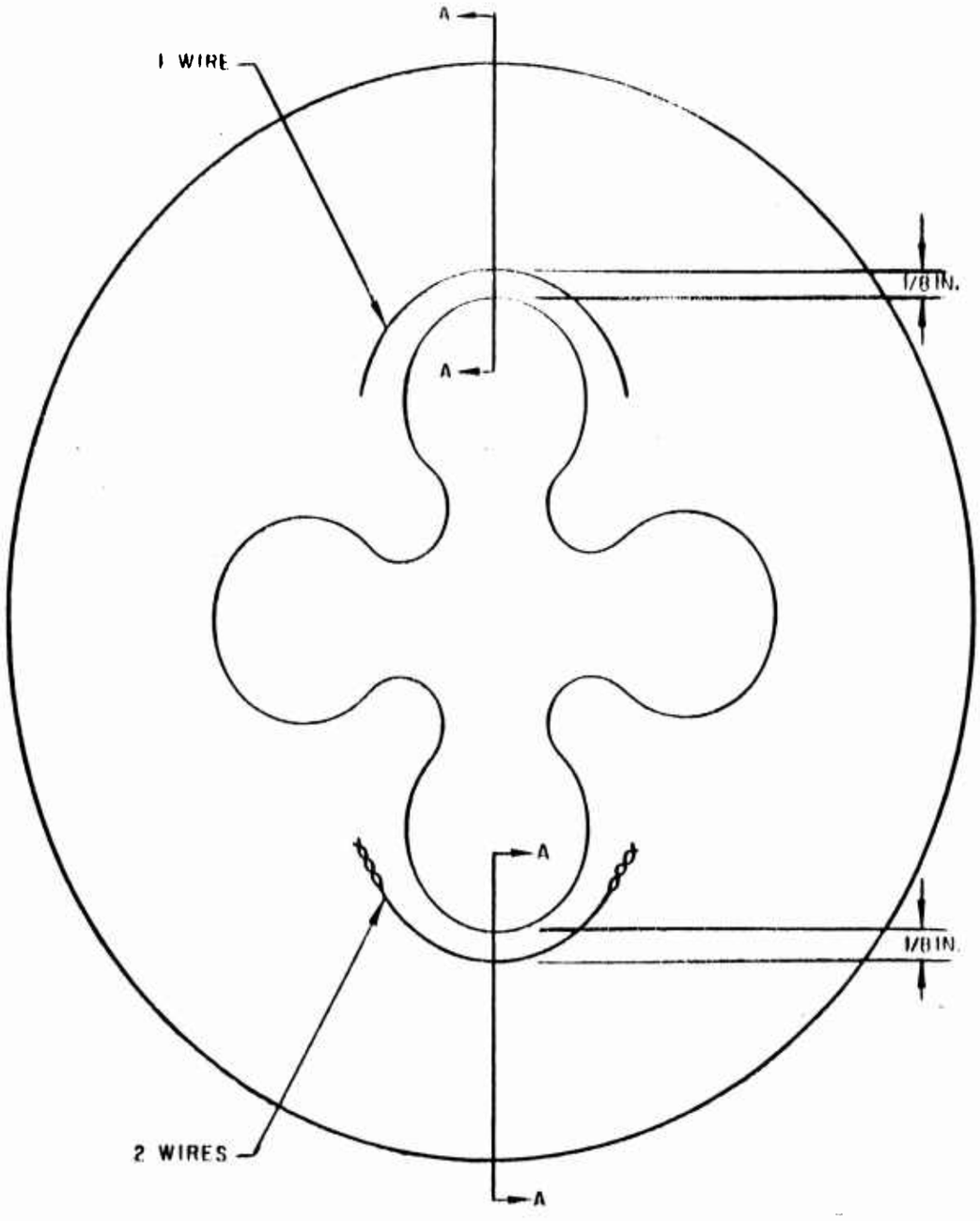

Fig. 3-17 Single and Double Wire Reinforced (Model No. 3)

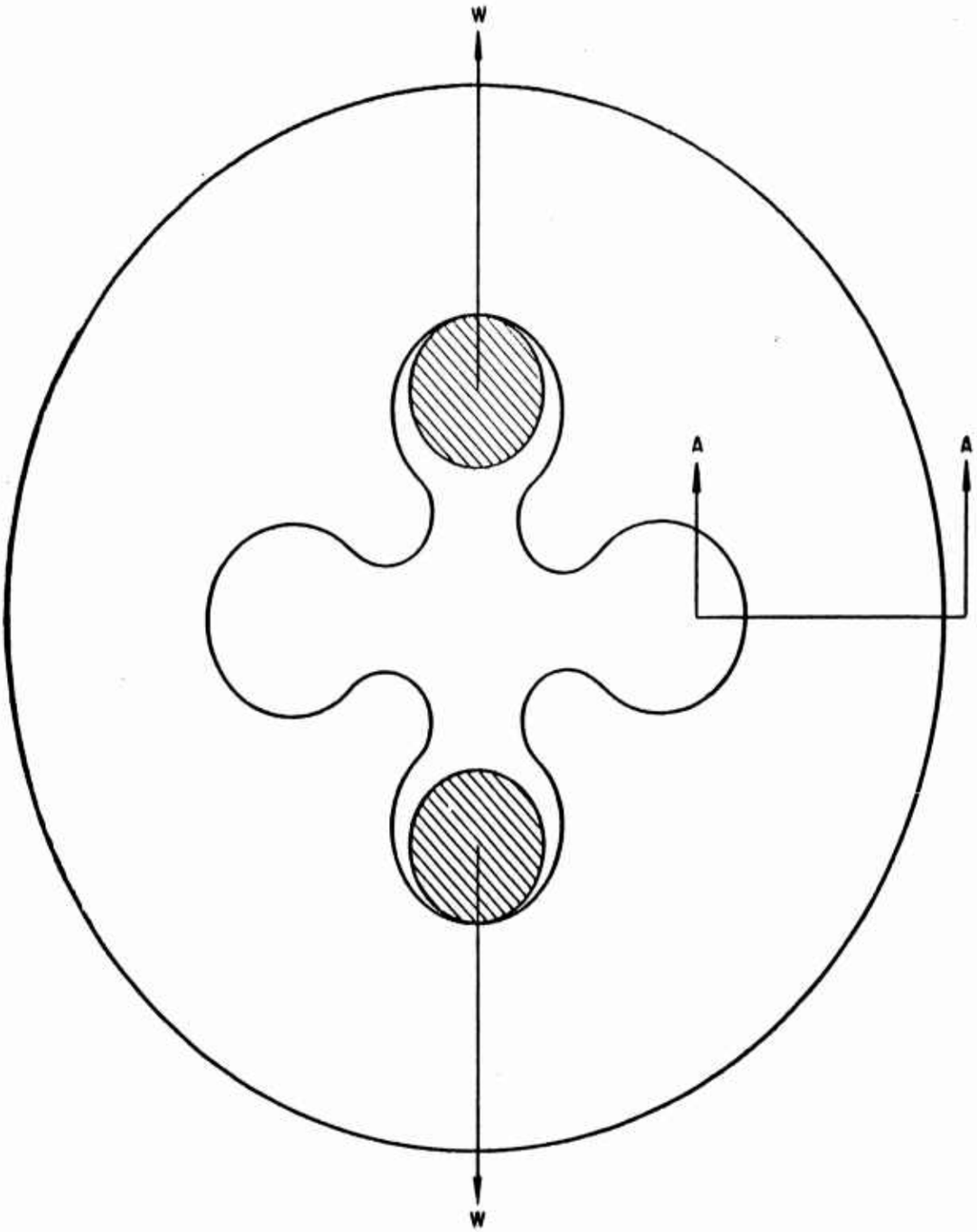

Fig. 3-18 Method of Loading and Section Analyzed (All Models)

larger than f_o, the stress at the outer edge (which is compressive). Also superimposed on this is a tensile stress across the entire section, but varying in intensity as shown in Fig. 3-20. Since the latter tensile stress is small compared to f_i due to bending, the result of the superposition is essentially the stress distribution shown in Fig. 3-19, except that there is a shift of the neutral axis away from the center of the model.

Under actual conditions, a propellant would be circumferentially reinforced against tensile stress similar in distribution to that shown in Fig. 3-20; and this tensile stress would arise from internal pressure or from shrinkage of the propellant within the metal casing to which it is bonded. These two conditions are difficult to reproduce on a model of the cross section; and these tests were intended merely to reproduce a peak of tensile stress (stress concentration) at the inner face of the cross section. The values of n' (or k) obtained from the diametrical loading test are not the same as those that would be obtained from a test correctly simulating the internal pressure. But the diametrical loading tests can be valuable in establishing trends and approximations.

Photostress was used to measure stress. With this technique, the models are coated with a birefringent plastic about 1/16-in. thick and observed at load under polarized light. Contours of constant "principal strain difference" appear as lines where red abruptly changes to blue; these contours are called "tints of passage" and are labelled F_1, F_2, F_3, etc. In the black and white photographs in this report, tints of passage appear as black lines or "fringes," while a black spot indicates a region of zero-stress. The first, second, and third lines beyond the black spot are the first, second, and third fringes, respectively. After the third fringe, the lines become fainter, and may not show up well in the reproductions. However, these reproductions have been included as they still illustrate the stress reduction which is due to reinforcing.

It is stated above that the fringe order is proportional to the difference in principal strains. At an edge, one of the principal strains is parallel to the edge and the other is zero; so, the fringe order is directly proportional to the non-zero principal strain.

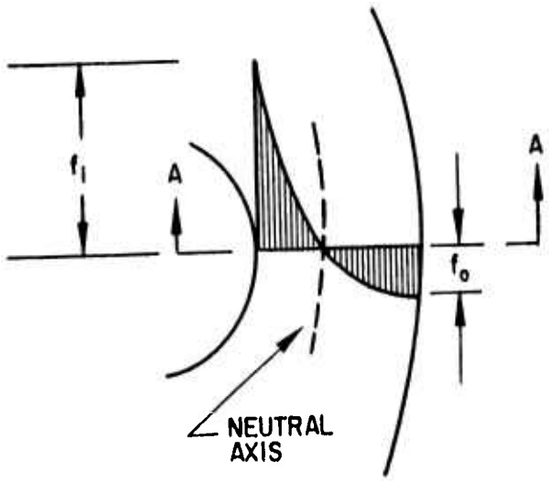

Fig. 3-19 Bending Stress at Section A-A

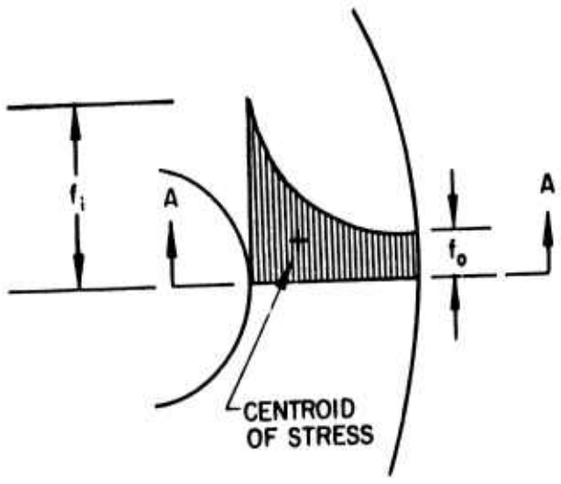

Fig. 3-20 Varying Tensile Stress at Section A-A

Also, where one of the principal strains is zero, and where the proportional limit has not been exceeded, the stress is directly proportional to the non-zero strain. Thus, in the following discussion, where only the inner edge at section A-A is considered, it is valid to discuss stress as being proportional to the fringe order.

For each of the three models, the diametrical load was held constant at 320 lb. In Fig. 3-21, which is a photograph of Model No. 1, locate either of the two sections A-A, then locate the midpoint of one of the sections A-A. Slightly toward the center (of the model) from the midpoint of section A-A, there is a black spot about 1/8 in. in diameter. This is a zero-stress point - technically, an "isotropic point" - and, for all intents, it occurs at the neutral axis (shown in Fig. 3-18) where the tensile stress changes to compressive stress.

As the observer looks at Section A-A and along a radial line from the zero-stress spot toward the center, he will see the first, second, third, and fourth fringes, F_1, F_2, F_3, and F_4, respectively, before encountering the inner edge of the model. Just beyond F_4, there is a thin strip of white which indicates that, at the inner edge, the circumferential stress magnitude is four plus some fraction.

In Fig. 3-22, which shows Model No. 2 (this model was also subjected to 320 lb diametrical load), only slightly more than three fringes can be seen.

In Fig. 3-23, two fringes are visible on both sides. On the left side, where there is only a single wire for reinforcement, a great deal of the lighter band that separates F_2 and F_3 (although F_3 is not present here) can be seen; while on the right side, where there are two wires for reinforcement, the second fringe occurs at the inner edge and none of the light band is visible. A visual estimate indicates that on the left there are two plus some large fraction of fringes, and on the right there are two or two plus some small fraction of fringes.

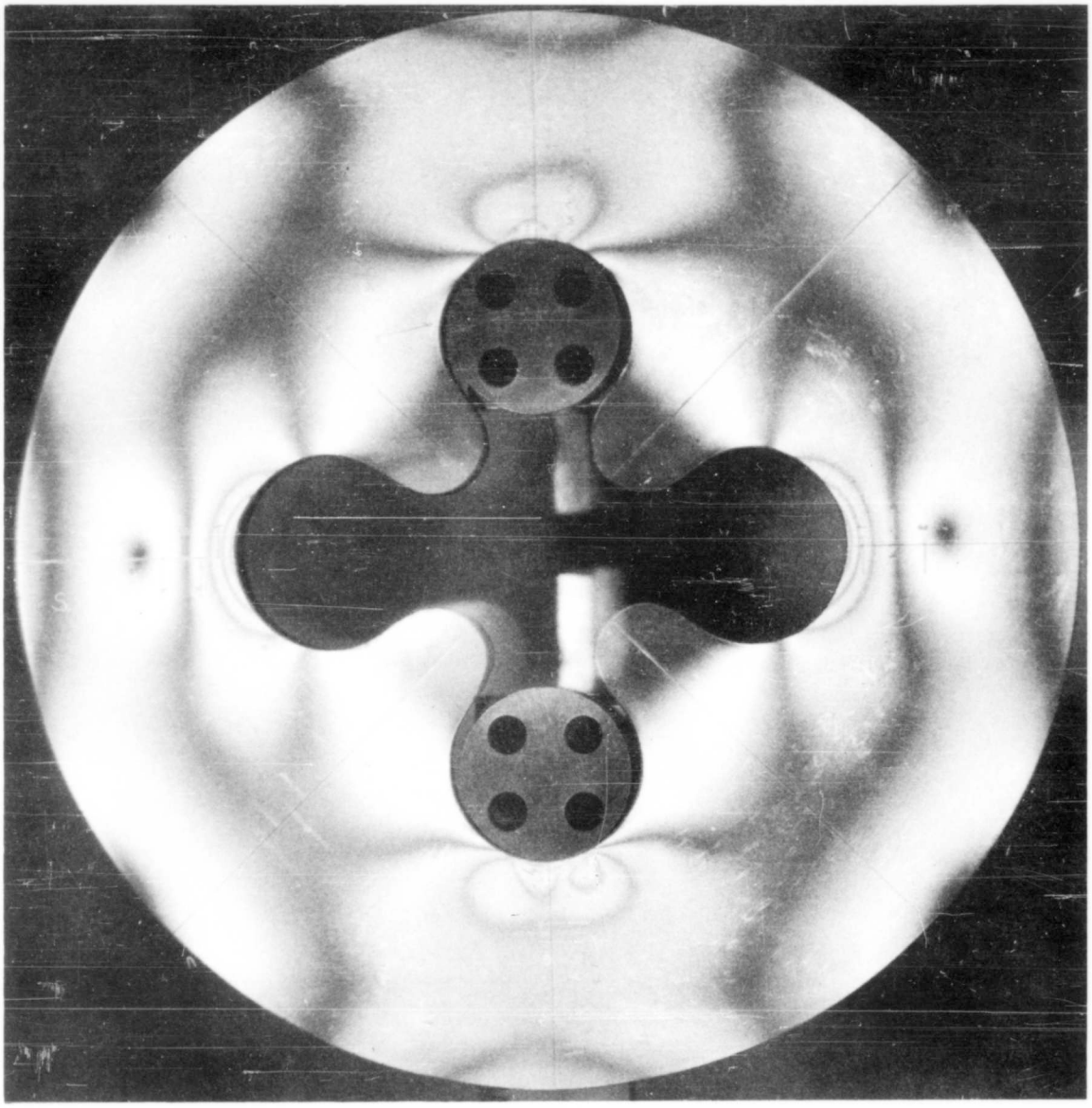

Fig. 3-21 Four-Pointed "Rounded" Star Under a Diametrical Load — Model No. 1: No Reinforcement

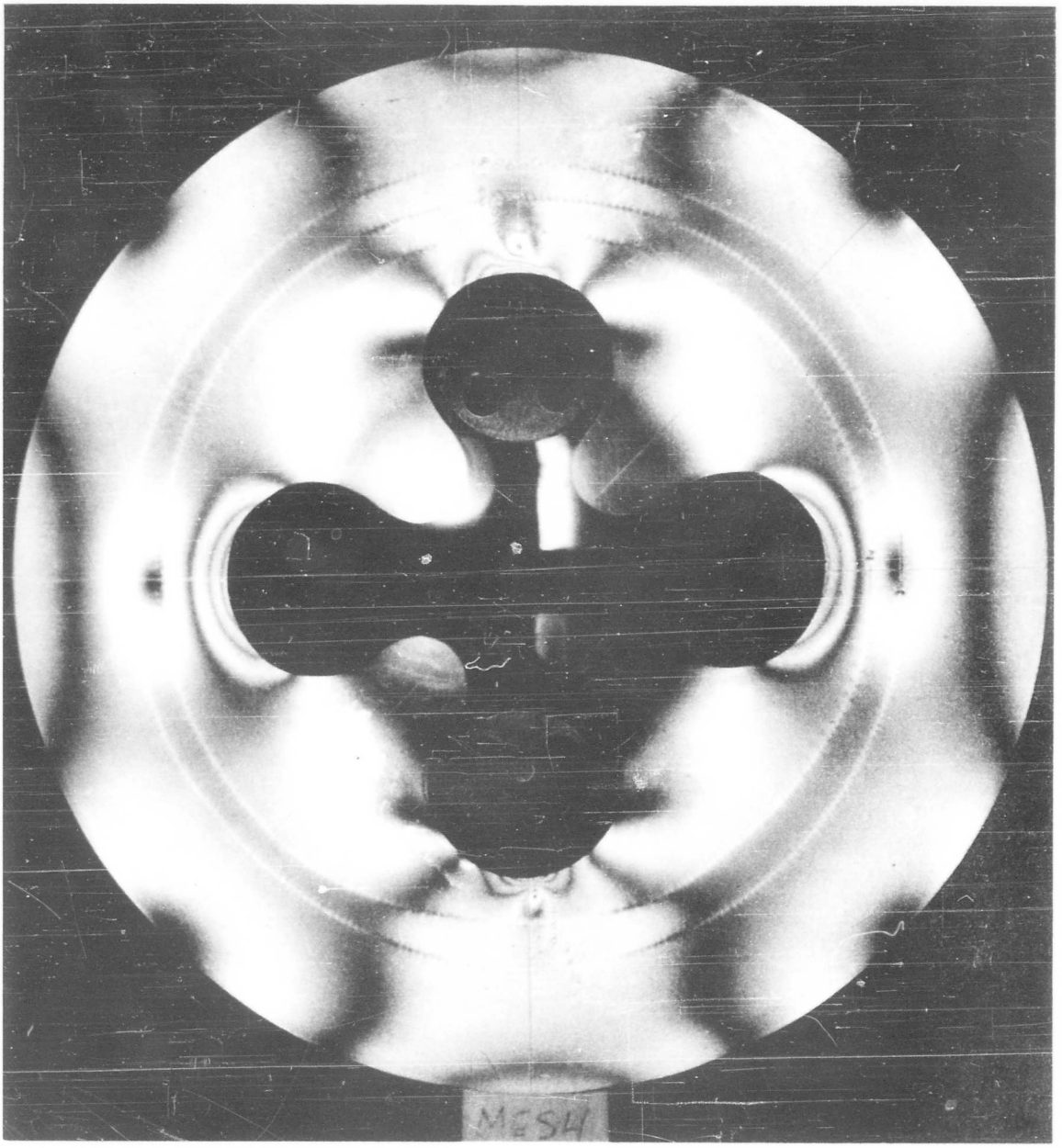

Fig. 3-22 Four-Pointed "Rounded" Star Under a Diametrical Load–
Model No. 2: Reinforced With a Spiral Wire Mesh

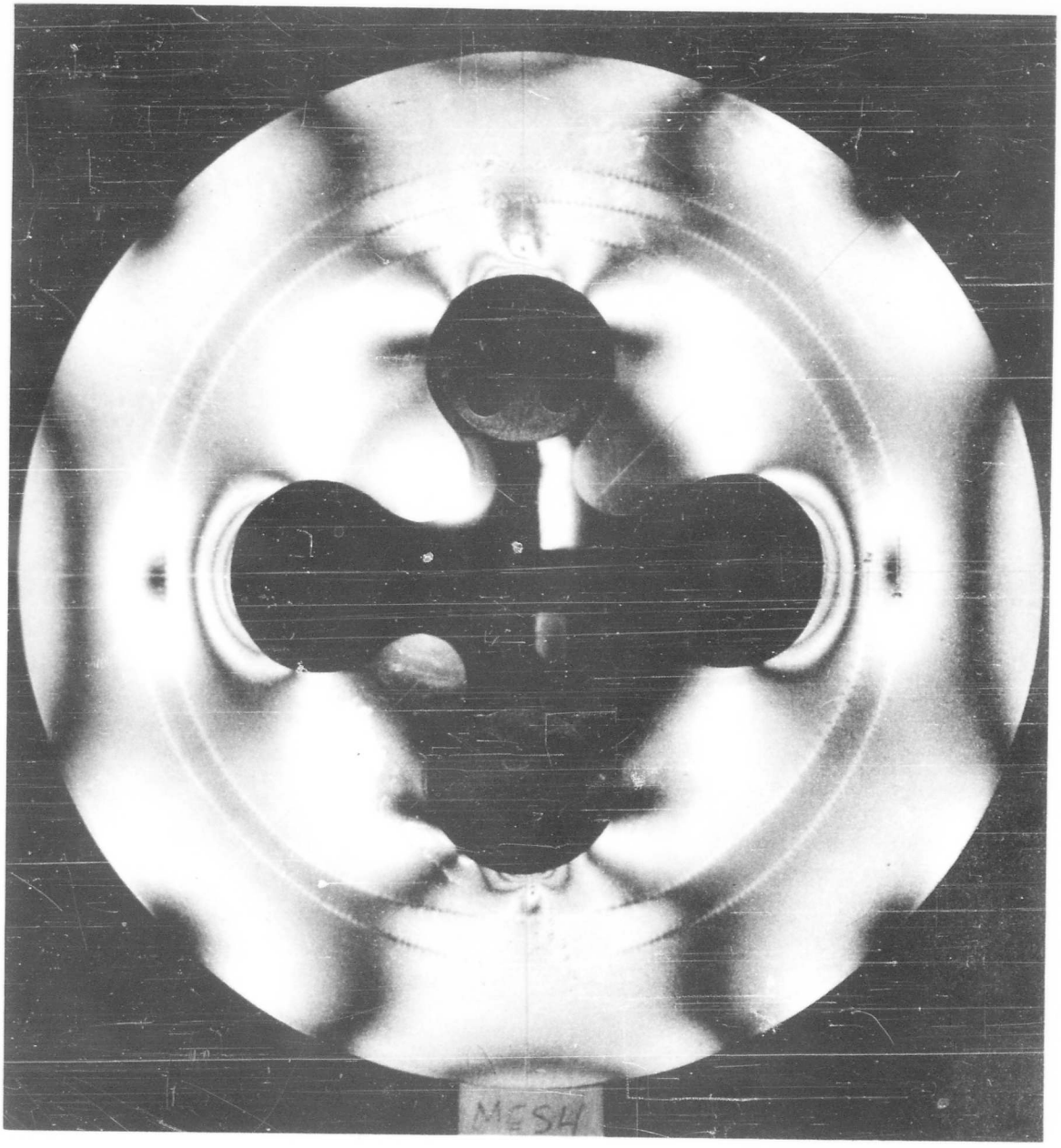

Fig. 3-22 Four-Pointed "Rounded" Star Under a Diametrical Load–Model No. 2: Reinforced With a Spiral Wire Mesh

The actual magnitude of the stress in each case is of no great interest. But the comparative magnitudes of stress in each model are significant. The visual estimates just described are usually accurate to one-fourth of one fringe (up to four fringes). Various instruments are available for more precise measurements. One such instrument, the LFZ Photostress instrument that uses goniometric compensation, produced the comparative stress magnitudes shown in Table 3-2. The accuracy of this instrument for this test is about 5 percent.

Table 3-2

COMPARATIVE STRESS MAGITUDES DETERMINED FOR REINFORCED MODEL PROPELLANT

Model No.	Figure No.	Type of Reinforcing	Comparative Stress Magnitude	Reinforcing Percent. P (%)	Reinforcing Benefit. B (%)	Experimental. k	Location of Neutral Axis	Location of Reinforcing Centroid
1	3-21	None	4.26	0	0	-	0.42d	-
2	3-22	Mesh	3.16	0.54	26	0.94	0.36d	0.30d
3	3-23 (left)	1 wire	2.82	0.66	34	1.11	0.33d	0.05d
3	3-23 (right)	2 wires	2.18	1.33	49	1.06	0.25d	0.05d

Table 3-2 lists the benefit B and the value of k obtained from the insertion of the appropriate values in the expression $k = \frac{B}{(1-B)(n-1)P}$, which is a transformation of Eq. (3.7a).

The location of the neutral axis expressed as a decimal of d, the depth of the section (1.50 in.) is also given in Table 3-2; thus, the neutral axis in Model No. 2 is 0.36 x 1.50 in. or 0.54 in. from the inner edge. The location of the centroid of the reinforcing is also given in the same fashion.

In Model No. 2, the centroid of reinforcing is very close to the neutral axis and the reinforcing is not subjected to much stress; this inefficient placement of the reinforcing produced an experimental value of k = 0.94.

In Model No. 3 (left side with the single-wire reinforcing), the area of reinforcing (or percent P) is increased a small amount from 0.54 to 0.67 percent, and yet the jump in benefit is considerable - from 26 to 34 percent. This increzse is mainly because of the shift in reinforcing centroid which produces a k of 1.11.

On the right side of Model No. 3, the reinforcing was doubled to two wires; the increase in benefit (from 34 to 49 percent) is not commensurate with the increase in P (from 0.66 to 1.33 percent) even though the reinforcing percent is still a small value (recall that n = 70, and refer to Fig. 3-3). But the addition of that much reinforces shifts the neutral axis inward (from 0.33d to 0.25d), and considerably reduces the effectiveness of the reinforcing. This example illustrates the diminishing returns condition that was mentioned in subsection 3.5. If the increase in reinforcing had not decreased k, the benefit would have been 52 percent instead of 49 percent.

For the materials used, the exact stress (±4 percent) can be determined by multiplying the comparative magnitude factors of Table 3-2 by 550, which gives the stress in psi.

3.10 PREPARATION OF SPECIMENS

All the models for this study were prepared from Epon 828 (100 pts.), using Lancast A (Ciba) (25 pts.) as the curing agent, and were cured at 85°C overnight. The specimen molds of the desired configuration were machined from Teflon or from aluminum. The aluminum molds were coated with a Teflon coating prior to use. Special precautions were taken during the casting step to minimize the voids in the models. Metals incorporated in the models were cleaned by procedures described in Section 2. (See Ref. 4.)

3.11 CONCLUSIONS

The following conclusions may be drawn from the structural analyses and tests performed in this study program:

- Reinforcing in a propellant grain can reduce stress due to loads; and since cracking is preceded by a tensile stress, reinforcing can reduce the tendency of brittle propellants to crack.
- Generally speaking, the extent of stress reduction due to reinforcing increases with increasing values of the ratio of the elastic modulus of the reinforcing to the elastic modulus of the propellant material.
- For simple bending and axial stresses (due to handling) the practical reduction in propellant stress due to reinforcing is about 75 percent, assuming that the propellant is not allowed to crack.
- For stress concentrations arising out of handling loads and internal pressure, the practical reduction in propellant stress due to reinforcing is about 50 percent.
- The orientation, location, and size of reinforcing is a very important factor. Reinforcing applied uniformly or randomly can be useless and even detrimental.

- Reinforcement with an expansion coefficient smaller than that of the propellant will cause tensile stresses in the propellant if the overall structure experiences a drop in temperature. This may limit the range of temperatures to which a reinforced propellant can be exposed, and may even make reinforcement impractical.

On the basis of these studies, it is evident that the introduction of structural elements into propellant grains to promote reinforcement of the grain may be beneficial in some respects but will also create special problems which have not previously been evaluated.

Section 4
DEVELOPMENT AND TESTING OF PROPELLANT GRAINS

4.1 INTRODUCTION

In order to achieve maximum impulse from a given solid fuel oxidizer composition, the amount of binder, almost invariably, must be reduced to about 10 percent of the total composition. This condition usually necessitates high-pressure forming methods to make the solids adhere to each other and to approach the theoretical density. The inclusion of structural elements in the propellant mass further complicates the development of forming techniques for making items such as burning-rate strands and motor grains for performance evaluation. The initial devices and procedures developed to cope with these problems are described in this section.

4.2 STRAND FORMING

Propellant strands of low binder content have been made successfully by isostatic pressing, a method employed industrially to form such items as carbon electrodes. Essentially, the method involves a sealed flexible envelope containing the power to be pressed. Air is removed from the envelope; then the envelope is placed in a hydraulic fluid to which pressure is applied, thus forcing the solid particles together.

In development work on strand forming, fuel-oxidizer mixtures were low enough in binder content so that they acted as free-flowing powders. These powders were tamped with mild pressure into a Teflon-lined rubber tube fitted with end plugs and a perforated cylindrical case (Fig. 4-1). Air was removed by pumping on both ends and screw clamps were used to seal off the tube. This holder was then placed in the hydraulic pressure vessel (Fig. 4-2), and pressure was remotely applied with a hand pump (Fig. 4-3). The perforated cylindrical case constrained the rubber tube against

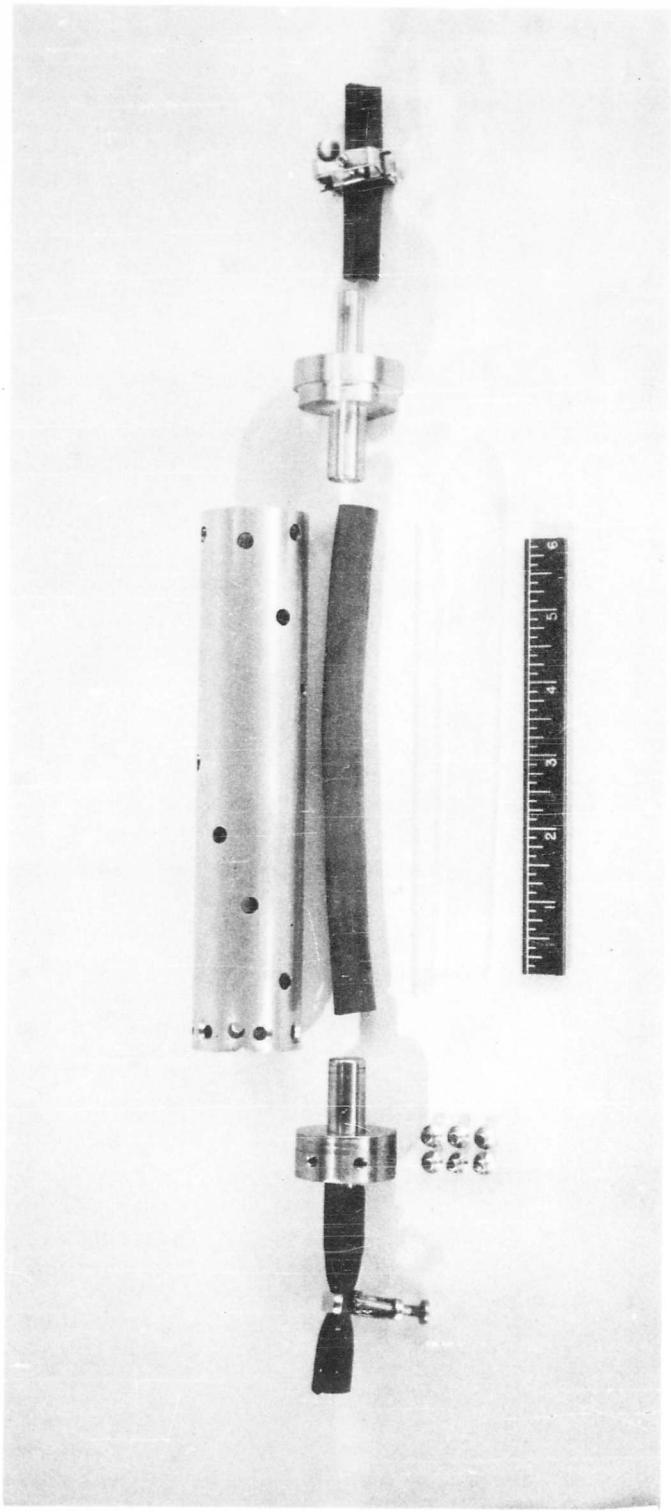

Fig. 4-1 Strand-Pressing Holder

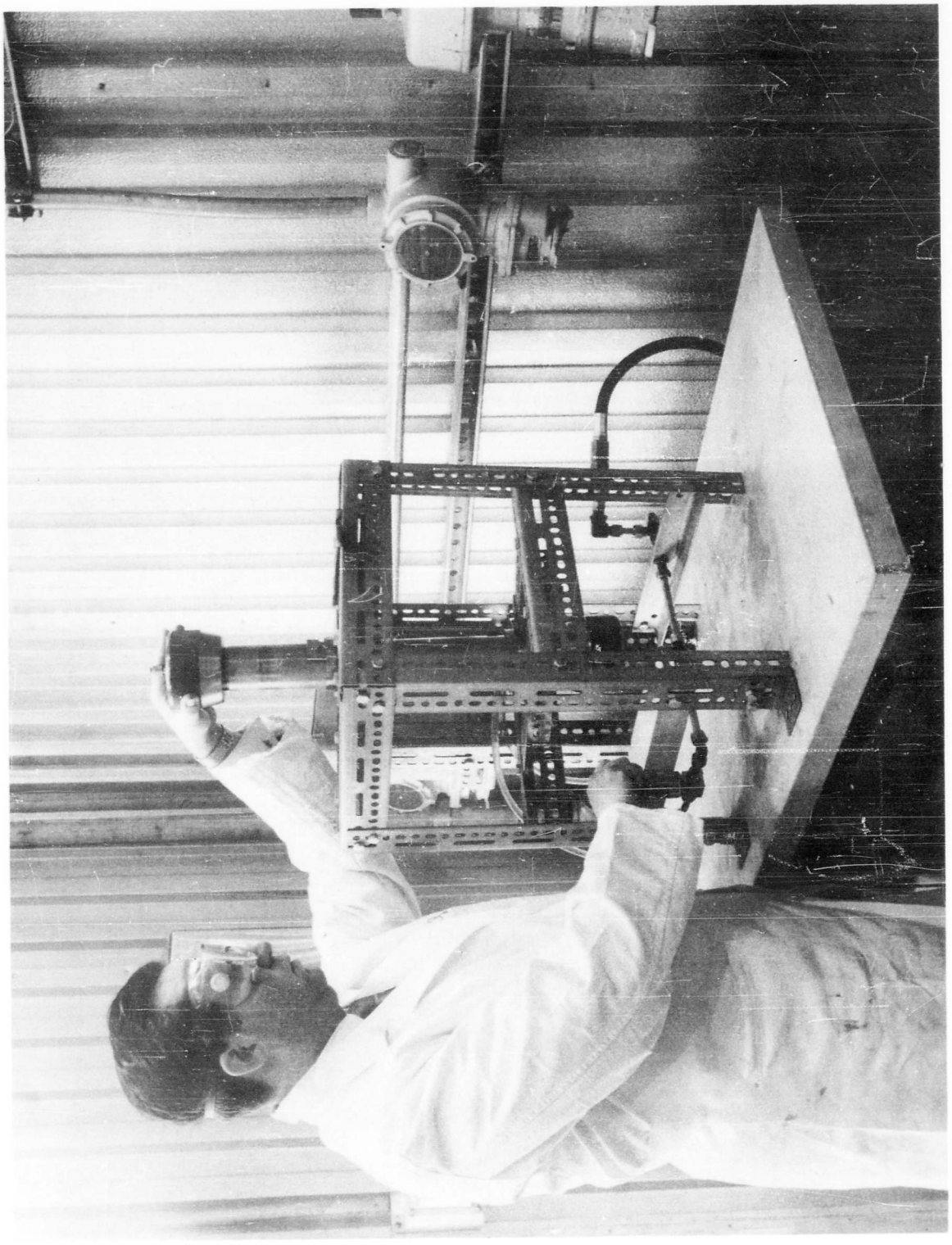

Fig. 4-2 Isostatic Pressure Vessel

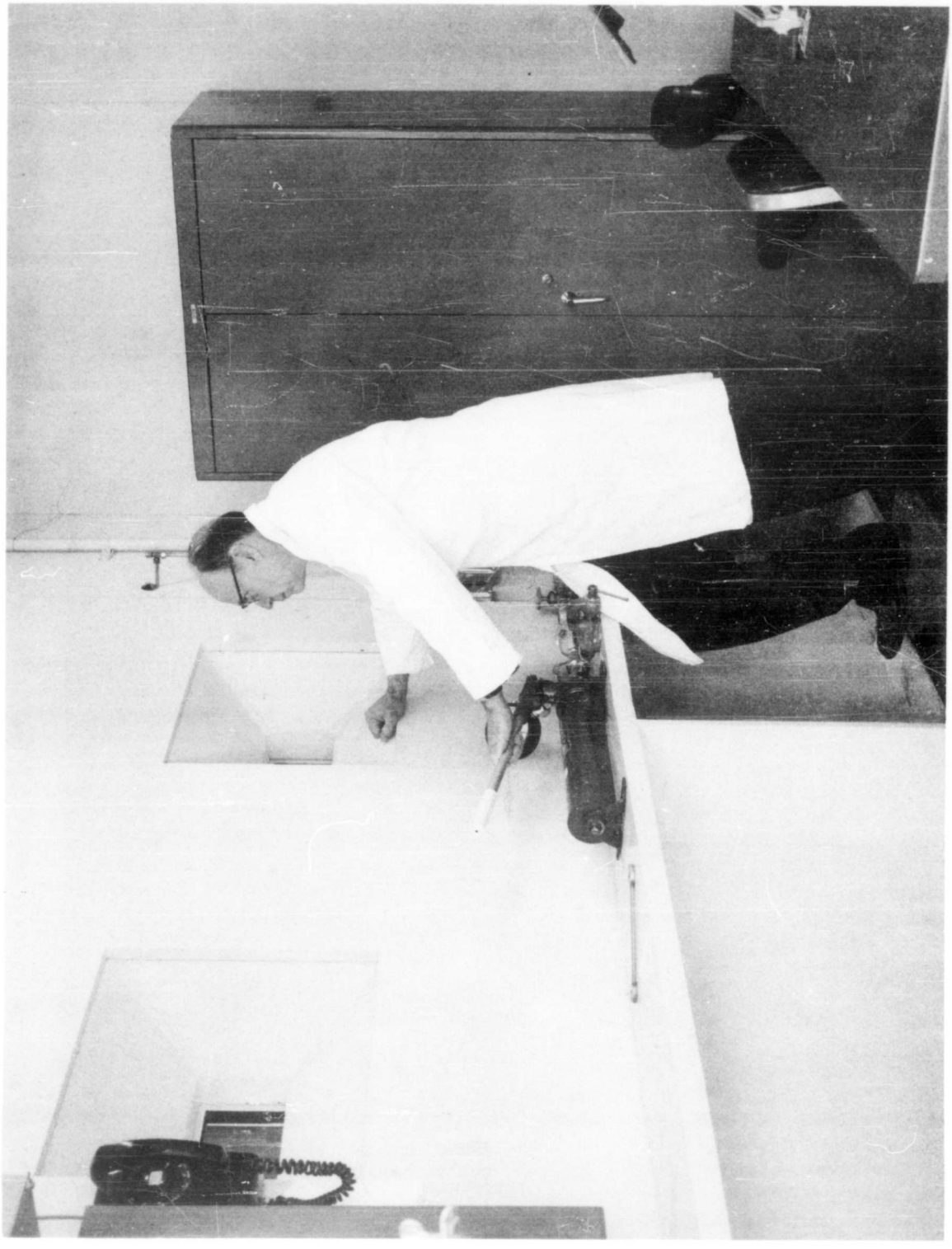

Fig. 4-3 Control Side (Building 627) Showing Hand Pump

longitudinal compressing. Pressures up to 10,000 psi were used. After removal from the press, the rubber tubes were cut off at the ends to permit removal of the pressed strand. Strands of about 5/16-in. diameter and 5 in. long were produced. No strands with structural elements were produced; but it is believed that with certain modifications such strands could be developed.

4.3 EXPERIMENTAL PROPELLANT-GRAIN FORMING

Forming grains from low-binder-content propellant powder presents many of the same problems, plus some additional ones, as those encountered in making strands. The characteristics of one propellant, for example, required an internal-burning grain. Furthermore, it appeared that forming the grain within the experimental motor case would simplify some of the difficulties involved in obtaining good bonding to the case.

The internal-burning motor grains were fabricated by first tamping the propellant powder into the annular space between the motor case and a centrally located tapered mandrel (Fig. 4-4). Eight equal increments were separately tamped using the hand pump (Fig. 4-3) in its remote position. Pressures between 3000 and 4000 psi were applied. The mandrel was then withdrawn using the upper hollow ram shown in Fig. 4-4, and a pulling rod which threaded into the top end of the mandrel. A specially designed rubber tube was then inserted in the hole left by the mandrel and a hydraulic pressure of 6000 psi or more was radially applied to the grain. Firm smooth grains of high density resulted. The embodiment of structural elements in grains formed by this technique has not yet been tried, but it is expected that certain configurations of these elements should work quite well.

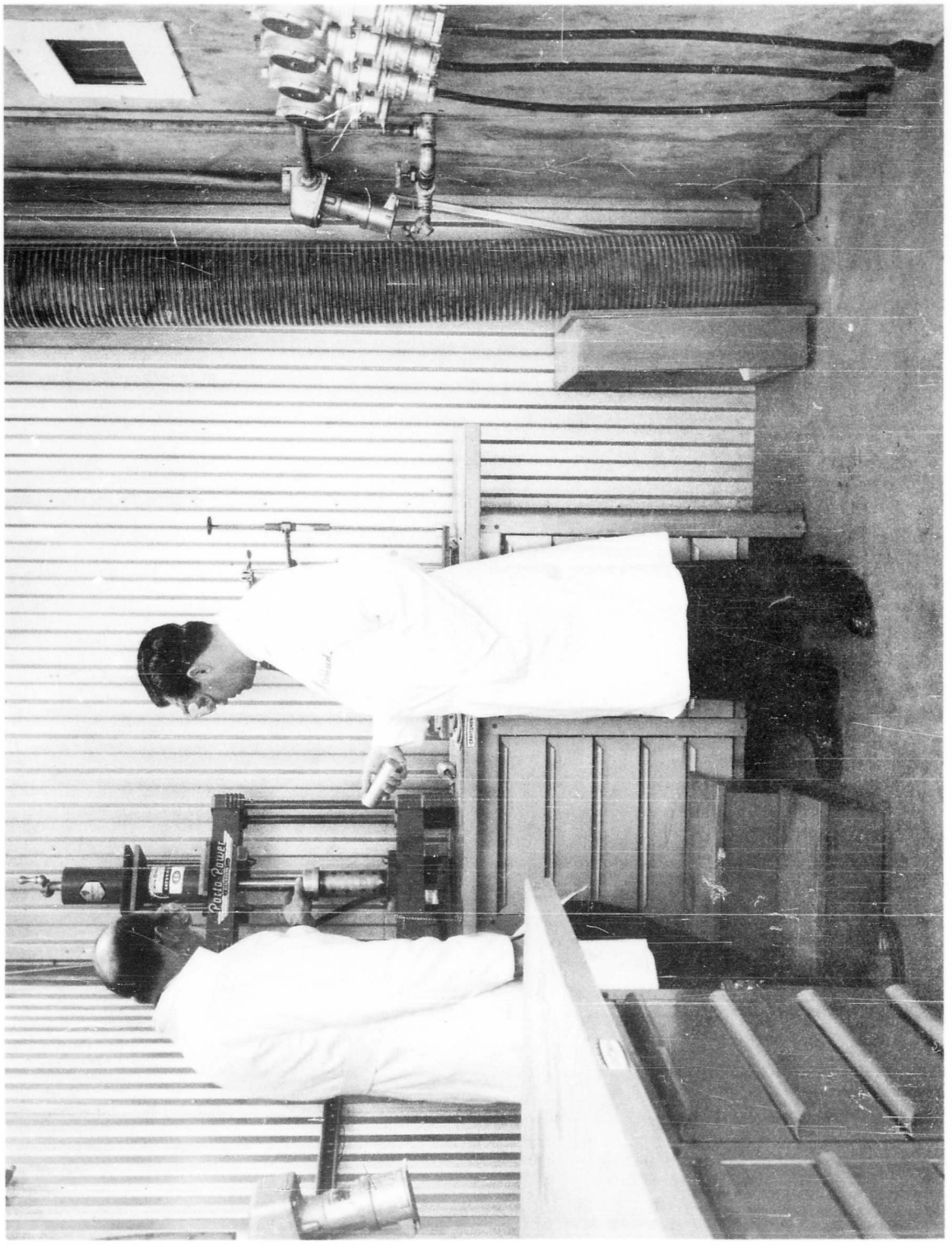

Fig. 4-4 Black Hawk Press (Operating Side of Building 627)

Appendix A
THEORETICAL ANALYSIS OF THE EFFECT OF METAL STRIPS ON THE BURNING RATE OF SOLID PROPELLANTS

A.1 SYMBOLS

a	constant coefficient in burning-rate equation; half width of the square cross section of the propellant (ft)
a_n	Fourier expansion coefficient
$\bar{a}$	constant
b	half thickness of metal strip (ft)
b_n	Fourier expansion coefficient
B	coefficient
c_n	Fourier expansion coefficient
c_p	specific heat of solid propellant (Btu/lbm °F)
h	convective heat transfer coefficient (Btu/hr ft^2 °F)
k_m	thermal conductivity of metal (Btu/hr ft °F)
K_n	ratio of burning surface to throat area
L	length of propellant strand (ft)
p_c	pressure of test chamber (psia)
q	heat flow (Btu/hr)
r	linear burning rate (in/sec))
R^*	defined as hL/k_m
t, T	temperature of metal strip (°F)
t_i, T_i	initial temperature (°F)
t_p	temperature of solid propellant (°F)
$\overline{t_p}$	average temperature of solid propellant (°F)
x	coordinate (ft)

y	coordinate (ft)
α	defined as $\frac{b}{B(a-b)} \frac{k_m}{\rho_p c_p}$ (ft^2/hr)
Γ	eigenvalue
σ	burning rate temperature sensitivity (in/in °F)
θ	time (hr)
ρ_p	density of solid propellant (lbm/ft^3)

A.2 INTRODUCTION

Solid propellant strands were prepared with a thin metal strip laminated into the strand along the direction of burning. In burning such strands, test results indicated a substantial change in burning rate for the propellant laminated with various metal strips of different thickness (Section 2). In this appendix, an attempt is made to analyze the transient heat transfer in the strand because of the metal lamination. The problem was treated as a metal strip heated at one end and conduction-cooled by the solid propellant on both sides. Although the present analysis is based on a fixed propellant-strand length (or the equivalent case of infinite length or near-zero burning rate), while in the actual case the length decreases with time, it at least provides some measure of the magnitude of the effects of heat transfer variation caused by different metal laminations and thicknesses.

A.3 ANALYSIS

This analysis is based on the following conditions:

- Propellant burning occurred at constant pressure.
- A perfect end-burning strand with negligible heat transfer from the entrapped combustion products in the test apparatus to the propellant strand is assumed.
- The combustion gas temperature is assumed to be constant.

- It is assumed that the temperature gradient in the propellant strand is small in the direction of burning, and that there is no heat flow in the propellant strand along that direction.
- The metal strip is assumed to be thin enough so that the heat capacity and temperature can be neglected.
- Thermal conductivity, the exposed area of the metal strip, and the convective conductance from the flame to the end of the metal strip are treated as constants.
- Heat transmission by radiation is neglected.
- The heat transfer from the flame front to the propellant through the propellant itself is not considered in the present analysis because the thermal conductivity of the propellant is small (a solid propellant is a good insulator) compared to that of the metal strip. Even if there were some heat conducted through the propellant from the flame front, the effect on burning would be about the same magnitude whether or not a metal strip is used. The present analysis deals with only the extra heat transfer through the metal strip lamination.

The burning of a solid propellant strand with a lengthwise metal lamination is shown in Fig. A-1.

An energy balance on an element of length dx and full cross section yields

$$q_x - q_{x\,+\,dx} = dq_y \qquad \text{(A.1)}$$

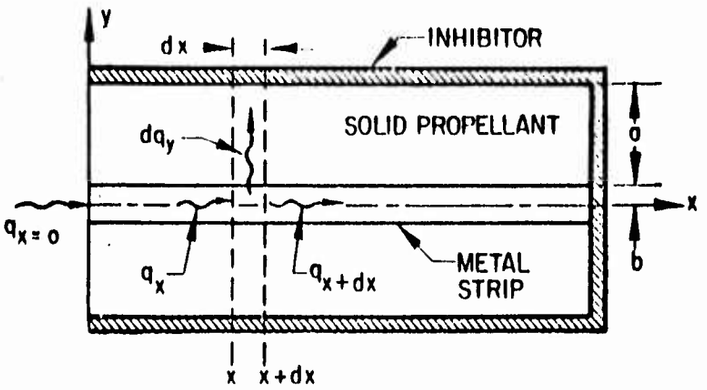

Fig. A-1 Heat Transfer Through a Metal Lamination in a Propellant Strand

The three rate equations involved are

$$q_x = -k_m (4ab) \left(\frac{\partial t}{\partial x}\right)_x \tag{A.2}$$

$$q_{x+dx} = -k_m (4ab) \left(\frac{\partial t}{\partial x}\right)_{x+dx} \tag{A.3}$$

$$dq_y = \rho_p c_p (4a^2 - 4ab)\, dx \frac{\partial \overline{t_p}}{\partial \theta} \tag{A.4}$$

where $\overline{t_p}$ is defined as the average temperature of this infinitesimally thin slab of solid propellant with thickness dx, i.e.,

$$\overline{t}_p = \frac{\int_b^a t_p dy}{a-b} \tag{A.5}$$

Also

$$\left(\frac{\partial t}{\partial x}\right)_{x\,+\,dx} = \left(\frac{\partial t}{\partial x}\right)_{x} + \left(\frac{\partial^2 t}{\partial x^2}\right) dx \qquad (A.6)$$

Substitution of Eqs. (A.2), (A.3), (A.4), and (A.6) into Eq. (A.1) yields:

$$\frac{\partial^2 t}{\partial x^2} = \frac{\rho_p c_p}{k_m} \frac{a-b}{b} \frac{\partial \overline{t_p}}{\partial \theta} \qquad (A.7)$$

Assuming that the typical temperature distribution in the propellant in the y direction is

$$\overline{t_p} = t\, e^{-\frac{y-b}{B(a-b)}} \qquad (A.8)$$

where B is a coefficient depending on propellant properties and temperature range, it can be seen (Fig. A-2) that as $\frac{1}{B} \rightarrow \infty$, for $y = a$, $\overline{t_p}$ approaches zero.

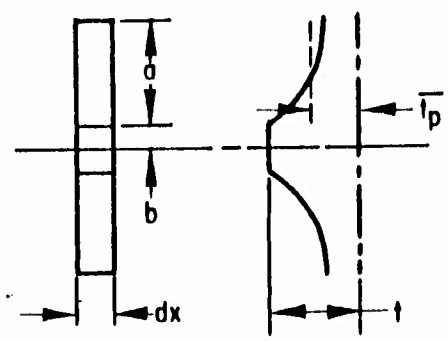

Fig. A-2 Typical Temperature Distribution in Solid-Propellant Strand

A combination of Eqs. (A.5) and (A.8) yields

$$\bar{t}_p = \frac{\int_b^a t\, e^{\frac{y-b}{B(a-b)}}\, dy}{a-b} \; Bt\left(1 - e^{-\frac{1}{B}}\right)$$

Since $\frac{1}{B} \to \infty$,

$$\bar{t}_p = Bt \tag{A.9}$$

The elimination of $\bar{t}_p$ in Eq. (A.7) by using Eq. (A.9) leads to

$$\frac{\partial^2 t}{\partial x^2} = \frac{\rho_p c_p}{k_m} \frac{B(a-b)}{b} \frac{\partial t}{\partial \theta}$$

Defining

$$\alpha = \frac{k_m}{\rho_p c_p} \frac{b}{B(a-b)}$$

then

$$\frac{\partial^2 t}{\partial x^2} = \frac{1}{\alpha} \frac{\partial t}{\partial \theta} \tag{A.10}$$

The intial condition is

$$\theta = 0 \;,\; t = t_i$$

For the boundary conditions,

$$(1)\;\; x = 0 \;,\; h(t_\infty - t) = -k_m \frac{dt}{dx}$$

and defining

$$T = t - t_\infty \quad , \quad \frac{\partial T}{\partial x} = \frac{\partial t}{\partial x} \quad , \quad T_i = t_i - t_\infty$$

then

$$hT = k_m \frac{dT}{dx} \tag{A.11}$$

$$(2) \quad x = L \quad , \quad \frac{dT}{dx} = 0 \tag{A.12}$$

Equation (A.10) can now be written as

$$\frac{\partial^2 T}{\partial x^2} = \frac{1}{\alpha} \frac{\partial T}{\partial \theta} \tag{A.10a}$$

The temperature of the metal strip as a function of x at various times is represented in Fig. A-3.

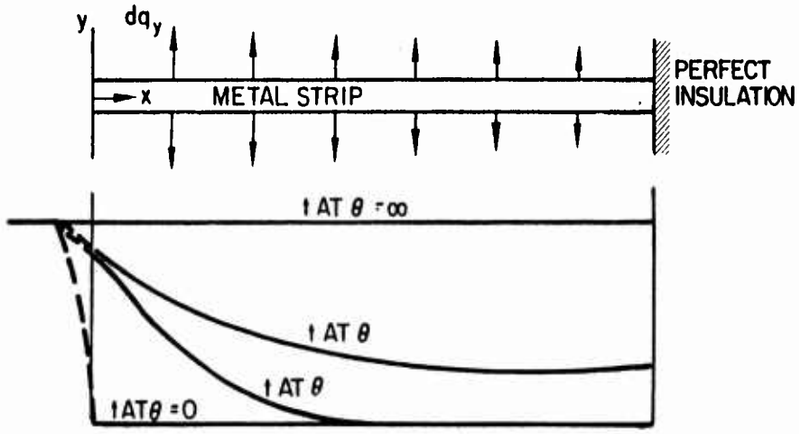

Fig. A-3 Expected Temperature Distribution Along the Metal Strip at Different Times

The solution of Eq. (A.10a) takes the form of

$$T = \sum_{n=1}^{\infty} e^{-\alpha \Gamma_n^2 \theta} \left[a_n \cos \Gamma_n x + b_n \sin \Gamma_n x \right] \qquad (A.13)$$

By introducing $a_n = c_n \cos \bar{a} \Gamma_n$ and $b_n = c_n \sin \bar{a} \Gamma_n$ into Eq. (A.13),

$$T = \sum_{n=1}^{\infty} c_n e^{-\alpha \Gamma_n^2 \theta} \cos \Gamma_n (x - \bar{a}) \qquad (A.14)$$

Now consider only the nth harmonic,

$$T_n = c_n e^{-\alpha \Gamma_n^2 \theta} \cos \Gamma_n (x - \bar{a})$$

and apply the boundary condition Eq. (A.12)

$$\frac{\partial T_n}{\partial x} = 0 \text{ at } x = L$$

$$\frac{\partial T_n}{\partial x} = - \Gamma_n c_n e^{-\alpha \Gamma_n^2 \theta} \cdot \sin \Gamma_n (L - \bar{a}) = 0$$

Since $\Gamma_n c_n e^{-\alpha \Gamma_n^2 \theta}$ cannot be zero for finite θ, $\sin \Gamma_n (L - \bar{a})$ must be zero.

Therefore,

$$L = \bar{a}$$

$$T_n = c_n e^{-\alpha \Gamma_n^2 \theta} \cos \Gamma_n (L - x) \qquad (A.15)$$

The second boundary condition may now be introduced.

At

$$x = 0 \ , \ \frac{\partial \Gamma_n}{\partial x} = \frac{h}{k_m} \Gamma_n$$

Consequently,

$$L \frac{h}{k_m} \cos \Gamma_n L = \Gamma_n L \sin \Gamma_n L$$

or

$$\frac{\Gamma_n L}{R^*} = \cot \Gamma_n L \qquad (A.16)$$

Equation (A.16) gives values of Γ_1, Γ_2, Γ_3,. . .,Γ_n. By applying the initial condition $T = T_i$ at $\theta = 0$ to Eq. (A.14) for all values of $0 \leq x \leq L$, then

$$T_i = \sum_{n=1}^{\infty} c_n \cos \Gamma_n (L - x)$$

By multiplying through by $\cos \Gamma_m (L - x) \, dx$, and undertaking a term by term integration in the interval $0 \leq x \leq L$,

$$\int_0^L T_i \cos \Gamma_m (L - x) \, dx = c_n \int_0^L \cos \Gamma_m (L - x) \cos \Gamma_n (L - x) \, dx \qquad (A.17)$$

or

$$\frac{T_i \sin \Gamma_m L}{\Gamma_m} = \frac{2c_n}{\Gamma_m^2 - \Gamma_n^2} (\Gamma_m \sin \Gamma_m L \cos \Gamma_n L - \Gamma_n \cos \Gamma_m L \sin \Gamma_n L) \qquad (A.18)$$

From Eq. (A.16),

$$\Gamma_n L \sin \Gamma_m L \cos \Gamma_n L = \Gamma_m L \cos \Gamma_m L \sin \Gamma_n L$$

Therefore, in Eq. (A.18), if $\Gamma_m \neq \Gamma_n$, the right-hand side vanishes. Hence, $\Gamma_m = \Gamma_n$ and Eq. (A.17) becomes

$$T_i \int_0^L \cos \Gamma_n (L - x)\, dx = c_n \int_0^L \cos^2 \Gamma_n (L - x)\, dx$$

The above leads to

$$c_n = \frac{T_i (2 \sin \Gamma_n L)}{\Gamma_n L + \sin \Gamma_n L \cos \Gamma_n L} \qquad (A.19)$$

Substitution of c_n and $\bar{a} = L$ in Eq. (A.14) yields an expression for the temperature of the metal strip as a function of time and distance from the flame front as follows:

$$T = \sum_{n=1}^{\infty} \frac{T_i (2 \sin \Gamma_n L)}{\Gamma_n L + \sin \Gamma_n L \cos \Gamma_n L} e^{-\alpha \Gamma_n^2 \theta} \cos \Gamma_n (L - x) \qquad (A.20)$$

By restoring t and t_i in Eq. (A.20), we get

$$\frac{t - t_\infty}{t_i - t_\infty} = \sum_{n=1}^{\infty} \frac{2 \sin \Gamma_n L}{\Gamma_n L + \sin \Gamma_n L \cos \Gamma_n L} e^{-\alpha \Gamma_n^2 \theta} \cos \Gamma_n (L - x) \qquad (A.21)$$

If it is assumed that the temperature of the not-yet-decomposed but preheated portion of the propellant δ distance (in the magnitude of micron) from burning surface controls the burning rate, then that temperature can be found by

$$t_{x=\delta} = t_\infty + (t_i - t_\infty) \sum_{n=1}^{\infty} \frac{2 \sin \Gamma_n L}{\Gamma_n L + \sin \Gamma_n L \cos \Gamma_n L} e^{-\alpha \Gamma_n^2 \theta} \cos \Gamma_n (L - \delta) \qquad (A.22)$$

The increase of burning rate can be found by

$$\sigma_p = \frac{1}{r}\left(\frac{\partial r}{\partial t_p}\right)_{K_n, p_c} \qquad \text{(A.23)}$$

A.4 DISCUSSION

This analysis is based on a fixed propellant-strand length or the equivalent of an infinite strand length or near-zero burning rate. For the nonfixed length, a step-by-step approximation is suggested, each calculated for a short period of time and different length L $[L = f(\theta)]$ and with temperature distribution in the metal strip as $T_i = f(x)$. The complication resulting from $T_i = f(x)$ is reflected in Eq. (A.17).

For infinite length and T_i = const, the partial differential equation (A.10a) with initial and boundary conditions $T = T_i$ and $hT\Big|_{x=o} = k_m \frac{\partial T}{\partial x}\Big|_{x=o}$ can easily be handled by using the Laplace transform. The final solution can be expressed as

$$\frac{t - t_i}{t_\infty - t_i} = \operatorname{erfc}\ \frac{x}{2\sqrt{\alpha\theta}} - e^{h\sqrt{\alpha\theta}/k_m\left(\frac{x}{\sqrt{\alpha\theta}} + \frac{h\sqrt{\alpha\theta}}{k_m}\right)} \operatorname{erfc}\left(\frac{x}{2\sqrt{\alpha\theta}} + \frac{h}{k_m}\sqrt{\alpha\theta}\right)$$

where erfc is known as the complementary error function and is defined as

$$\operatorname{erfc} X = 1 - \operatorname{erf} X = \frac{2}{\sqrt{\pi}} \int_X^\infty e^{-\lambda^2}\, d\lambda$$

The error function expression is easier to deal with than Eq. (A.22) in which a tedious computatation might be encountered if the series does not converge rapidly.

It is predicted that a metal with high thermal conductivity would provide a high burning rate if the same heat transfer coefficient h exists for all conditions. However, h

may vary significantly if a phase change in the metal is involved, especially in the case of liquid to vapor. Test results indicated that the burning rates with different metal strip laminations are in the order of brass, aluminum, and steel. The thermal conductivities and melting points of the three metals are given in Table A-1.

Table A-1

THERMAL PROPERTIES OF CERTAIN METALS

	Yellow Brass	Aluminum	Steel
k_m, thermal conductivity (Btu/ft-hr °F)	9.4	13.6	10
Melting point (°F)	1710	1120	2600
Boiling point (°F)	4700 (for copper)	4530	4890

The higher burning rate with aluminum strip over steel strip can be explained by the differences in k_m. The reason brass lamination burned faster than aluminum can not be explained without resorting to the differences in the melting and boiling points, and in turn, the difference in the heat transfer coefficient h.

An increase in the thickness of the metal lamination should always be accompanied by an increase in the burning rate on the condition that the burning surface is not significantly reduced by the area taken up by the metal.

Since the heats required for melting, boiling, and combustion of the laminated metal were not considered in the analysis, these factors might be the explanation for the test result where the burning rate leveled off as the thickness of steel strip increased.

The idealization of constant thermal conductivity may not be valid, especially in the high-temperature regions.

Because of temperature variation across the propellant strand (y direction), the burning surface will be in a reversed wedge shape shortly after burning starts. The pressure distribution along the curved surface will also affect the burning rate.

A.5 CONCLUSIONS

The present analysis, starting from a transient approach, predicts the effect of laminations with different metals on the burning rate as a function of (1) nondimensional parameter $R^* = \frac{hL}{k_m}$ (where h is the heat transfer coefficient from gas to metal, L is the instantaneous length of the propellant strand, and k_m is the thermal conductivity of the embedded metal), (2) the properties of the solid propellant, and (3) the relative dimensions of the metal strip to propellant. The validity of the analysis needs to be substantiated by experimental data. The information on the thermal conductivity of metals at high temperatures and on the heat transfer coefficient for various metals under different flow and phase change is meager or lacking, and therefore, further investigation and experimentation are required. The energy involved in bringing the metal lamination to melting, boiling, and combustion should be included in the future analysis. In addition, an extension of the present theoretical analysis to the case of nonfixed strand length and different configurations of metal strips is recommended.

Appendix B

THEORETICAL BURNING CHARACTERISTICS OF STRANDS CONTAINING METAL STRIPS

Conventional propellant strands exhibit a flat burning surface normal to the longitudinal axis. If a metal strip is placed in the center of the strand as shown in Fig. B-1, the apparent burning rate or propagation rate along the longitudinal axis r_2 increases.

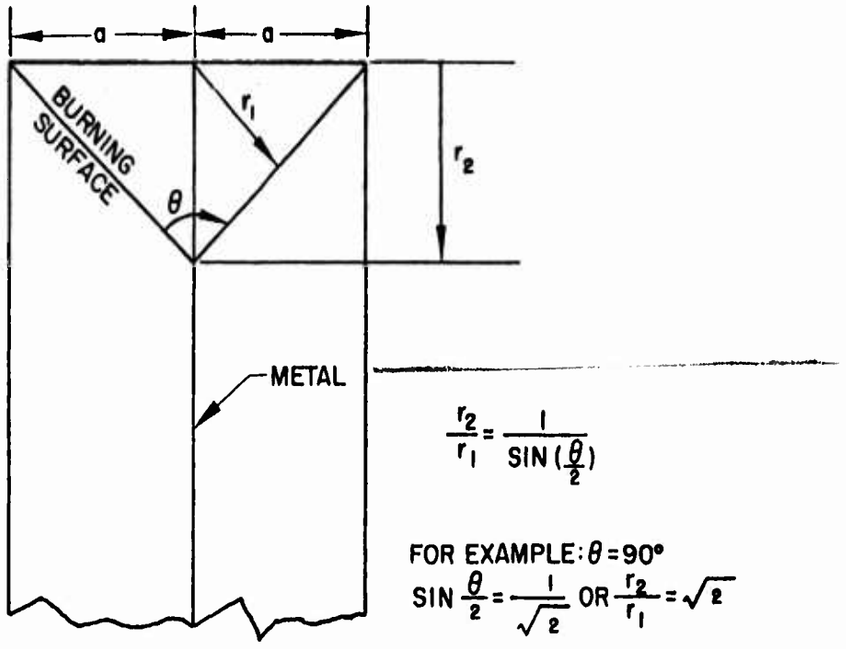

Fig. B-1 Geometry of Burning Surface of Propellant Containing Metal Strip

If we assume that the burning rate, normal to the propellant surface r_1 remains constant, two relationships can be simply derived.

- The ratio of the burning rates r_2/r_1 varies as a function of the angle θ at the metal-propellant interface. This relationship, easily obtained from Fig. B-1, is $r_1/r_2 = \sin(\theta/2)$. A plot of the function is shown in Fig. B-2.

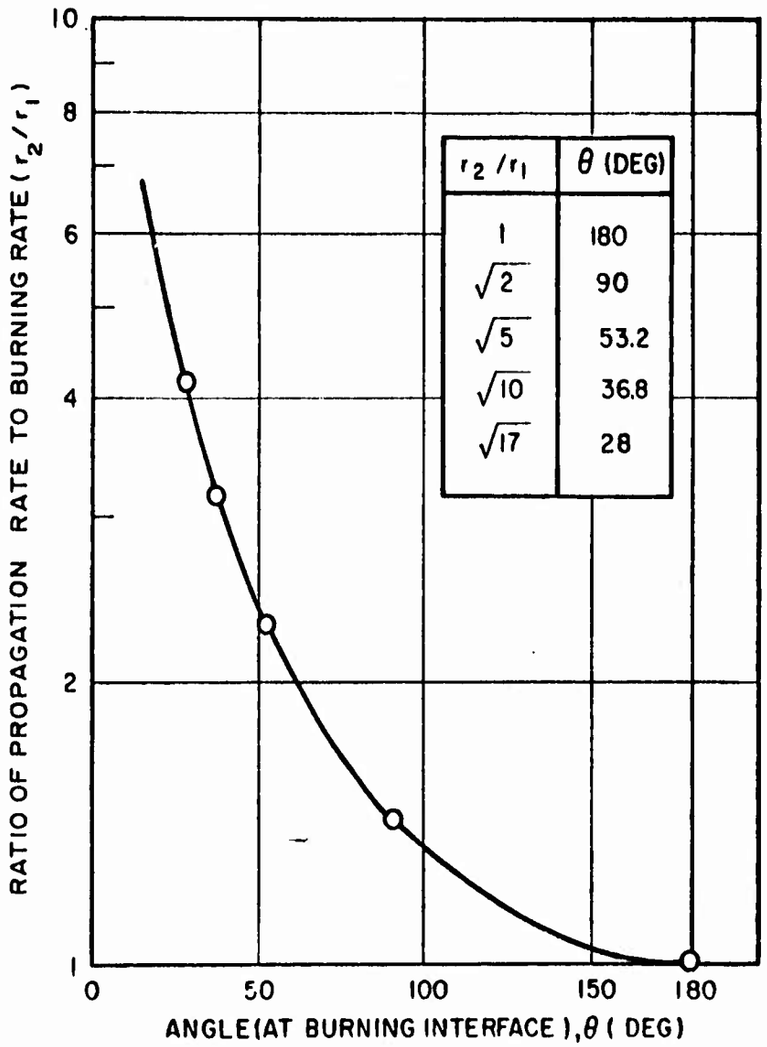

Fig. B-2 Ratio of Burning Rates Versus Angle at Metal Interface

- The ratio r_2/r_1 is also dependent upon the cross section of the propellant, that is, the distance a on each side of the metal strip. The greater the distance a, the smaller the apparent burning rate r_2 for a given r_1, as indicated in Fig. B-1.

A verification of the angle relationship and burning rates would require photographic techniques. Effects of metal thickness, configurations other than the simple monolaminate, and type of metal can also be evaluated.

Appendix C

SUMMARY OF BURNING-RATE DATA

Table C-1

SUMMARY OF BURNING RATES FOR PROPELLANT STRANDS CONTAINING METAL STRIPS

(FORMULATION I) [a]

Metal	Thickness (mils)	Burning Rate (in /sec)			
		325 (psi)	500 (psi)	750 (psi)	1000 (psi)
None	-	0.19	0.26, 0.25, 0.28, 0.25, 0.24	0.21, 0.32	0.26, 0.22, 0.25
Aluminum	1.2	-	0.50, 0.51, 0.49	0.53	0.63, 0.56
Aluminum	7.1	0.50	0.56, 0.56 0.60	0.63, 0.65	-
Aluminum	10.9	-	0.60	0.62	0.71
Stainless Steel	2.2	-	0.34, 0.36	0.36	0.41
Stainless Steel	6.2	-	0.30, 0.32, 0.33	-	0.38
Stainless Steel	9.7	0.22	0.30	0.34	0.36

[a] Ratio of NH_4ClO_4 to Aluminum – 62/38; see Table 2-1.

Table C-2

SUMMARY OF BURNING RATES FOR PROPELLANT STRANDS CONTAINING METAL STRIPS

(FORMULATION II)[a]

Metal	Thickness (mils)	Burning Rate (in /sec)			
		325 (psi)	500 (psi)	750 (psi)	1000 (psi)
None	-	0.21, 0.19	0.24	0.26, 0.24 0.23	0.29
Aluminum	1.2	0.47	0.50	0.55	0.59[b]
Aluminum	7.1	0.58	0.61	0.73	
Stainless Steel	2.2	0.34	0.40	0.50	
Stainless Steel	6.2	0.24	0.28	0.39	
Brass	2.5	0.56, 0.68	0.68	0.78	
Brass	6.6	0.70	0.83	0.83	

[a] Ratio of NH_4ClO_4 to Aluminum – 85/15; see Table 2-1

[b] Test conducted at 900 psi

UNCLASSIFIED